TECHNISCHE UNIVERSITÄT MÜNCHEN

ABSCHLUSSARBEIT IM MASTERSTUDIENGANG KERN-, TEILCHEN- UND ASTROPHYSIK

Effect of Stellar Rotation on the Dark Matter Capture Rate

Anja Brenner

supervised by
Prof. Alejandro IBARRA

7. Februar 2019

Abstract

So far, the rotation of the stars around their own axis was not considered in the formula for the dark matter capture rate. We modify the previously used capture formalism for the non-relativistic case by taking into account the rotation of stars. We want to find out how this affects the dark matter capture rate in the sun and in an O-B-star. Furthermore, we want to predict how this change in the capture rate influences the cross section limits from IceCube, where the influence on the sun is important, and the stellar evolution of so-called Dark Stars, where the influence on O-B-stars near the galactic center plays an important role. Considering dark matter masses from 100 GeV to 10 TeV, we determine the change in the capture rate for the rotating case. We find out that the capture rate in case of the sun is not significantly influenced by considering rotation. This also means that the cross section limits of IceCube remain unchanged. The effect on the O-B-star is very small, $\approx 1\%$. This leads to very small changes in the stellar evolution which is hardly detectable.

Acknowledgements

First and furthermore I want to thank my supervisor Prof. Alejandro Ibarra for his help during the project and inspiring discussions. Furthermore, I want to thank my family and friends for their support during my studies. Special thanks also go to Andreas Rappelt for useful discussions.

Contents

1. Introduction

Investigating the anisotropies in the Cosmic Microwave Background (CMB), gravitational lensing effects or rotation curves of galaxies it becomes clear that there must be another source of gravitational interactions, apart from visible matter. A promising way to explain the unexpected result is that our universe is filled with invisible matter, so-called dark matter (DM). DM interacts via gravitation. Apart from that, we know e.g. that DM has to have a long lifetime in cosmological timescales, it had to be non-relativistic at the structure formation time and it interacts at most weakly via other forces. One of the main questions is, what is the nature of the DM, or whether there is even more than one kind of DM particles acting in the universe. There is a numerous number of models that include a DM candidate. A promising DM candidate is the weakly interacting massive particle (WIMP) since the cross section between DM and Standard Model (SM) particles essentially determines the freeze-out time, which in turn essentially determines the relic DM abundance. By choosing a cross section that is comparable to the weak cross section, the predicted DM abundance is in the region of the measured one. The measurements indicate that visible matter makes up roughly 5 % and DM about 25% of the total energy amount in our universe. The remaining 70% are made of dark energy.

Since the coupling between WIMPs and nuclei is non-zero, there is a chance to detect them in direct detection experiments. In principle, this means that DM particles could interact with nuclei in a detector and transfer energy to them. This recoil energy can be measured if it exceeds the energy threshold of the detector, but we will not look into this detection method in this work.

Another method to detect DM is indirect detection. Here, products of DM annihilation, e.g. neutrinos, can be detected in detectors on the earth.

But also Dark Stars (DSs) can act as instrument for DM detection. DSs look like ordinary stars, but they are powered, at least for a while, by the annihilation of the contained DM. To accumulate DM particles in the core of the star, an important process is the capture of DM particles traversing the star. This capture process is well studied and the effect of DM annihilation on stars has already been elaborated. But up to now, the rotation of the stars around their own axis was not considered. The goal of this work was to rewrite the capture formalism by considering the rotation of stars and to give an outlook about how a change in the capture rate influences previous analyses in particle and astrophysics. Therefore, we arranged this work as follows.

In chapter 2, we briefly motivate DM, especially WIMPs, introduce DSs and describe Ice-

Cube. In the beginning of chapter 3, we present the previously used DM capture formalism. After that, we derive two approaches for the DM capture rate where the stellar rotation is considered. In chapter 4, we show the results for the modified DM capture rate formalism. In the following chapter, we draw conclusions and in chapter 6, we give an overview of what the next steps can be in order to improve this work. In the end of the chapters 2 and 3, we added a short summary with the essential information of the particular chapter in order to help the reader keep the perspective. Finally, we complete this work with the appendices.

2. Basics

2.1. General information about dark matter

In this section, we briefly give the most important information about DM which includes the evidence of its existence, the short introduction of an appropriate DM candidate and in the end DM detection.

2.1.1. Evidence for dark matter

In 1932, the Dutch astronomer Jan Hendrik Oort studied the vertical motion of stars near the galactic disk to determine the acceleration of matter [1]. Using the star density and the velocity dispersion of the stars, he obtained information about the gravitational potential of the Milky Way. The result was by no means in line with the expectations: The inferred potential turned out to be not strong enough to hold the stars bound to the disk. But with the galaxy appearing stable, there must either be matter near the galactic plane which was not observed, or - as Oort conjectured - gravitational attraction behaves differently. This was one of the first hints for the possible presence of DM.

In 1933, the Swiss astronomer Fritz Zwicky studied the redshift of various galaxy clusters and found that there was a large scatter of the apparent velocity dispersion ($\approx 2000\,\frac{km}{s}$) in eight galaxies within the Coma Cluster [2]. He tried to determine the mass of large clusters of galaxies using the virial theorem [3] and came to the conclusion that the dynamic mass should be at least a hundred times larger than that of the luminous matter. This led Zwicky to conlude that most of the matter has to consist of non-luminous matter.

Zwicky's prediction of the fraction between the dynamic and luminous matter turned out to be overestimated. However, his conclusion that there must be more DM than luminous matter has been confirmed by others. Today, it is known that the composition of matter in galaxy clusters like the Coma Cluster is as follows: 85 % DM, 14 % hot intracluster medium (ICM) and 1 % stars [4]. It has been found that not only galaxy clusters but also individual galaxies are dominated by DM, even dwarf galaxies.

During the years, several hints for DM occured. In the following, we list and briefly explain the most important ones.

CMB anisotropies

In the early universe, baryonic matter was exposed to two counteracting forces, gravitation and radiative pressure. These counteracting forces generated oscillations, the so-called Baryonic Acoustic Oscillations (BAO). In overdense regions, baryonic matter was thus compressed by gravity and forced apart by the photon pressure. DM, on the contrary, only interacts gravitationally and therefore remained, unaffected by the photon pressure, in the center of the density accumulations. After decoupling, the photons no longer interacted with the baryons and propagated away, leaving behind a baryonic shell. These photons we nowadays see as the CMB.

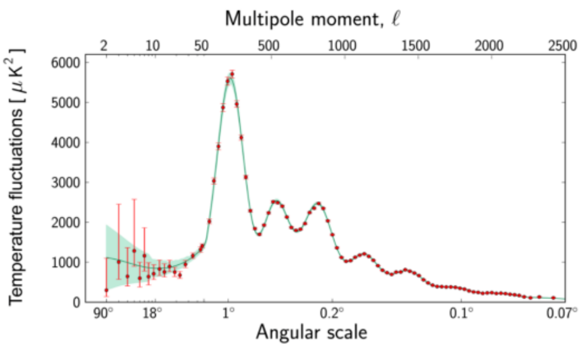

Figure 2.1.: CMB power spectrum of temperature fluctuations in the cosmic microwave background. The fluctuations appear at different angular scales in the sky. The green curve represents the Standard Model of cosmology, ΛCDM. The red dots with the error bars represent the Planck data. The figure was taken from [5].

In figure 2.1 the CMB power spectrum is shown. The power spectrum characterizes the size of the density fluctuations as a function of angular scale.

The first peak corresponds to size of the density fluctuations which fully compressed once before the decoupling of the photons. So the position of the first peak gives the horizon at that time. With this information one can conclude that the universe has a flat or nearly flat geometry, because the expected size of the horizon at the time of recombination fits well with the angluar size of the first peak.

From the first three peaks we can also calculate the density of baryonic matter and the total matter in the universe. The total matter density defines the amplitude of the peaks in the CMB power spectrum and the baryonic matter defines the ration between the odd and even peaks, which correspond to full compression and decompression at the time of recombination, respectively . To explain the CMB power spectrum most of the matter in the universe has to be dark, non-baryonic matter. According to Planck [6] and WMAP [7], there is five times more DM than baryonic matter in the universe.

Bullet Cluster

The Bullet Cluster consists of two galaxy clusters that collided some time ago. The stars which were contained in the two clusters were hardly affected during the collision. They moved almost unhindered through the center of the collision, so that they are still located in the respective clusters as before the collision. Only the movement was a little slowed down by gravitational interactions.

The situation is different by investigating the ICM, which can be well observed by the emitted X-rays. The gas, which makes up the majority of baryonic matter, interacts electromagnetically. As a result, the movement of the ICM was very much slowed down at the collision region of the two galaxy clusters. Examining the emitted X-rays of the gas, one realizes that most of the baryonic matter is lagged behind the location of the gravitational matter.

If one compares this result to the result of gravitational lensing, whereby the distortion of objects in the background of the clusters were examined, large discrepancies were found. From the latter, it can be seen that most of the matter is still in the respective cluster as before the collision. How the two clusters look now, after the collision, is illustrated in figure 2.2. As one can see, the gravitational matter does not coincide with the baryonic matter.

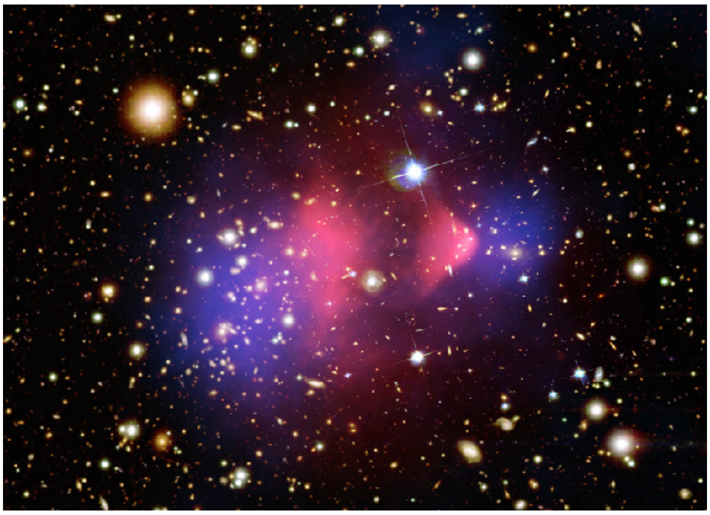

Figure 2.2.: Image of the bullet cluster taken by the Chandra X-ray observatory. The picture shows a collision of two galaxy clusters. The baryonic matter is illustrated in pink, whereas the gravitational matter is blue. The latter consists mostly of DM, but also of stars and gas. The picture is taken from [5].

One way to interpret this observation is the following: The galaxy clusters consist not only of stars and the ICM but also of DM which propagates unhindered, similar to the stars, through the collision and does not, in contrast to the ICM, slow down [5].

Rotation curves of galaxies

If we measure the velocity of stars at different distances to the center of the galaxy, we obtain the rotation curve of the galaxy. With it we can learn something about the mass distribution in the galaxy. In theory, the velocity of stars far away from the center should behave as $v_c \sim r^{-\frac{1}{2}}$. This result is obtained by equating the Newtonian gravitational and centripetal forces. But theory and observations contradict each other. According to the results of the velocity measurements, the velocity of the stars far away from the galactic center behaves like $v_c \approx$ constant. From this we can conclude that mass still grows with the distance, even though the amount of luminous matter decreases with the distance to the galactic center. This is shown in figure 2.3.

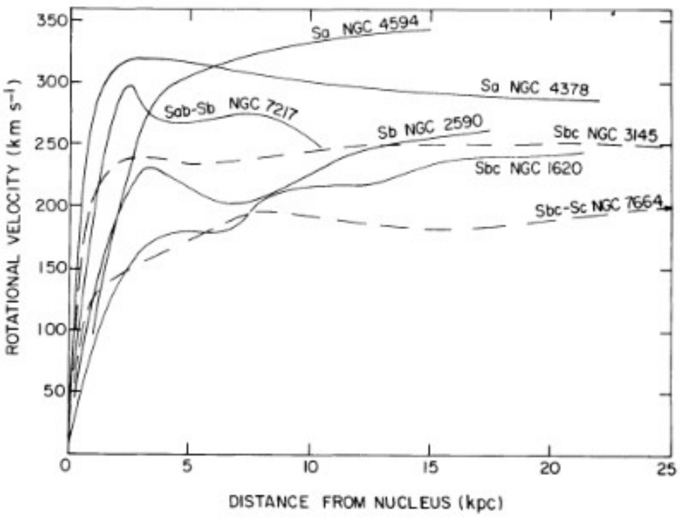

Figure 2.3.: Rotational velocity of seven galaxies for various distances between galactic center and star as shown in [8]

This missing observed mass can be explained by the presence of DM [8].

2.1.2. The WIMP as dark matter candidate

The nature of DM is still unknown, but in order to explain the evidences in the previous subsection, a DM candidate has to fulfill several requirements.

- It interacts at most weakly via other forces than gravitation. Otherwise one could detect it easier.
- It has to be stable in cosmological timescales. The lifetime has to be at least the age of the universe.
- It reproduces the observed DM density of $\Omega_\chi \, h^2 \sim 0.1$.

A DM candidate which fulfills these conditions is the weakly interacting massive particle (WIMP). As the name indicates, it interacts only weakly and besides, it is stable in cosmological timescales. One way to generate the DM abundance is the so-called freeze-out mechanism. Here, the DM and Standard Model (SM) particles were in thermal equilibrium in the very early and hot universe. At that time, the DM particles converted into the lighter SM particles and vice versa via interactions like DM + DM $\leftrightarrow$ SM + SM. As the universe expanded, and therefore cooled down, the SM particles no longer had sufficient energy to produce the heavier DM particles. In addition, the density of the DM particles decreased and at some point, it was too low to interact frequently so that their comoving number density remained constant. One sais that the particles "froze-out".

One can write the expression for the today's DM abundance in terms of the thermally averaged annihilation cross section times the relative velocity of the interacting particles $< \sigma\, v >_{ann}$. It then takes the form [9]

$$\Omega_\chi \, \mathrm{h}^2 \sim \frac{10^{-26} \, \frac{cm^3}{s}}{< \sigma\, v >_{ann}} \tag{2.1}$$

where h denotes the Hubble constant in units of 100 $\frac{km}{Mpc\, s}$. Assuming weak scale interactions for the DM candidate, i.e.

$$< \sigma\, v >_{ann} \sim \, 10^{-26} \, \frac{cm^3}{s}, \tag{2.2}$$

one obtains the correct DM abundance $\Omega_\chi \, \mathrm{h}^2 \sim 0.1$ [10]. This coincidence is called "WIMP miracle".

Depending on their freeze-out time or rather their freeze-out temperature, one furthermore distinguishes between three types of DM candidates. If the temperature at the freeze-out time was smaller than the mass of the DM particle, one is speaking of cold DM. These particles are non-relativistic. Hot DM describes DM particles whose mass was lower than the temperature at the freeze-out time. These particles are relativistic. The properties of warm DM candidate are in between the ones of hot and cold DM. From observations we have learnt that cold DM would lead to the observed large scale structures via the bottom-up scenario [11]. Bottom-up scenario means that small structures form first before they accumulate to larger ones. So e.g. galaxies form first and merge then to clusters of galaxies. In simulations, hot DM leads to a top-down scenario which does not result in the large scale structures observed today.

Since cold DM fits the observations best and the WIMP fulfills the requirements mentioned above, we assume in the following that DM is described by WIMPs moving with non-relativistic velocities.

2.1.3. Dark matter detection

Although the existence of DM is able to explain big physical puzzles, like the rotation curves of galaxies, many properties of DM are not known so far, e.g. the mass. Several experiments want to determine these properties.

The basic idea of direct detection experiments is the following. DM particles enter the detector and scatter off the detector material elastically. In this collision, the DM particle transfers energy to the target particle. The recoil energy of the target particle will be measured if it exceeds the threshold of the detector. Since other particles like electrons and neutrons could also produce such a signal, it is an additional challenge to filter out the background. Experiments that use this kind of detection method are e.g. PandaX-II [12], LUX [13], CRESST II [14], XENON1T [15], and PICO [16].

While the detector material in direct detection experiments is supposed to interact directly with the DM particles, the material in indirect detection experiments does not react with the DM particles themselves but with particles produced by annihilation or decay of DM particles. Examples for indirect detection experiments are IceCube [17, 18], ANTARES [19], Baikal NT200 [20], and SuperK [21, 22]. which are looking for neutrinos produced by the annihilation or decay of DM particles.

Current observations are well consistent with the expected background and do not show evidence for DM annihilations or decays. However the experiments have set limits on the cross section. The best limits for the SD interaction for DM masses of 100 GeV and 10 TeV come from IceCube, namely $\mathcal{O}\left(10^{-41}\,\mathrm{cm}^2\right)$. The best limits for the SI interaction come from XENON1T. The limit for $m_\chi = 100$ GeV is $\mathcal{O}\left(10^{-46}\,\mathrm{cm}^2\right)$ and for $m_\chi = 10$ TeV it is $\mathcal{O}\left(10^{-45}\,\mathrm{cm}^2\right)$. IceCube is also described in more detail in section 2.3.

There are other possibilities to confirm the presence of DM apart from the evidences mentioned in 2.1.1, namely by using astrophysics. If there is for example DM accumulated in the center of the star, it influences the stellar evolution. Capture of DM in stars is important for the DM accumulation. The capture formalism for DM was already developed about 30 years ago [23]. Up to now, one always assumed for the calculations that stars are non-rotating objects. This was one of the main motivations for this thesis, namely to see how the rotation of stars can affect the DM capture and therefore how it changes the previous assumption of the stellar evolution.

2.2. Dark Stars

As mentioned before, one field where DM capture could play an important role is star formation and evolution.

The star formation process works as follows. Molecular clouds fragment and collapse due to local instabilities in these clouds. The product of this collapse is a protostar, with an opaque and pressure supported core, in hydrostatic equilibrium, which is still consuming mass from the surrounding molecular cloud. Stars in hydrostatic equilibrium compensate the energy loss due to radiation by contraction which follows the virial theorem. For gravitational systems, the virial theorem is

$$< V >= -2 < T > \tag{2.3}$$

where $< T >$ is the average total kinetic energy and $< V >$ is the average total potential energy. A consequence of the contraction is the continuous rise of the temperature in the core. If the temperature reaches a certain value, the Zero Age Main Sequence (ZAMS) stage of the star starts. In this stage, hydrogen fusion sets in which powers the star. For a more detailed explanation of the theory of stellar evolution see [24].

But the presence of DM inside the star can affect this formation process (and also the further evolution). An example for stars whose formation process and evolution is influenced by DM are the so-called Dark Stars (DSs) [25].

DSs are stellar objects like ordinary stars, but at some time they are powered by an exotic process besides nuclear fusion: heating due to annihilation of accumulated DM particles in the core of the DS. The annihilation products which are trapped inside the star, such as photons and electrons, scatter off nuclei in the star and energy is injected into the system. So, the star is heated as a consequence of DM annihilation.

One has to be careful with the expression "heating" since it can be misleading here. A star is a gravitating object and does though not meet the exact definition of thermodynamic equilibrium. That is the reason that stars have a negative heat capacity. In reverse, that means that if energy is injected into the star's system, its temperature decreases. This temperature decrease in turn leads to a suppression of the hydrogen burning. Since the age of a star is characterized by its stage of nuclear fusion, the suppression of the nuclear burning slows down or even stops the aging process for that time, depending on the strength of the temperature decrease. In the meantime, the star can accrete more mass from its environment and can grow even bigger.

Besides the usage of the term 'Dark Star' as a designation for stars that are temporarily powered by DM annihilation, it can also be used as designation for the new stellar phase that accumulated DM can enforce, namely the fueling of the star by DM annihilation. In which way the term 'Dark Star' is used becomes clear from the context.

Before we investigate the evolution of stars which can be influenced by DM annihilation, we briefly list and explain the criteria that have to be fulfilled for DS heating.

2.2.1. Criteria for Dark Star heating

Not every star which contains DM in its core is dominated at some time by DM heating. For this, the following criteria must be fulfilled [26]:

High DM density inside the star

The energy generated by annhilation is higher when the DM density in the core is high, since the produced energy $Q_\chi \propto \rho_\chi^2$. There we can see that the released energy by the annihilation process scales with the square of the DM density inside the star, ρ_χ. The reason for the quadratic dependence is that two DM particles always have to go together for an annihilation. So the annihilation becomes very important in regions with a high DM density.

Especially in the first stars, annihilation could have been a powerful energy source, because of the high DM density inside. There are four reasons for the high values:
1) The DM densities were higher by $(1 + z)^3$ with the redshift z.
2) The first stars formed in the center of DM halos where the DM density was very high compared e.g. to the one in the solar vicinity today.
3) Due to the quasi-static contraction of the protostar, the DM profile was compressed further [27].
These first three reasons refer to the formation of the DS where DM adiabatically contracted contemporaneously to the contraction of the star.
4) Efficient DM capture can increase the DM density in the star as well.
The fourth reason is another possibility to increase the DM density even after the formation process.

DM annihilation products trapped inside the star
If the annihilation products would not be trapped inside the star, the energy produced by annihilation would be carried out of the star. The heating rate is $f_Q\, Q_\chi$ per unit volume where f_Q describes the fraction of annihilation energy which is deposited into the gas. The annihilation products and their energy depend on the WIMP model. If one assumes the W^+W^-- decay channel for the DM annihilation, one gets $f_Q \sim \frac{2}{3}$.

If these criteria are fulfilled, the star can be powered at some time by DM annihilation. Since the conditions for DM heating have been clarified, we can now investigate the evolution of the star and the different contributions to the luminosity of the star.

2.2.2. Dark Star formation and life

To fulfill the criteria from the previous section, it is necessary to fill the star with DM. There are two possibilities how DM can get inside the star.

The first possibility is important during the star formation. When a star forms it follows the process described in the beginning of this section. The present DM in the molecular cloud contracts simultaneously to the baryonic matter. When the contraction is advanced enough, so that the DM density in the star is sufficiently high, DM annihilation of the contracted DM can become efficient. This means that the DM annihilation powers the star. Due to this, the contraction of the star is stopped for a while. After a certain time, the DM fuel runs out, contraction continues and nuclear burning sets in.

At that time, the second possibility to fill the core of the star with DM can become important, because the number density of the nuclei in the star is sufficiently high. Then DM capture can become efficient. Here, some of the DM particles which are travelling through the star scatter off the nuclei in the star. If the DM particles lose enough energy so that their velocity after the collision is smaller than the escape velocity at the scattering point, they become gravitationally bound to the star. Considering multiple scattering, they can even lose more energy and accumulate at the center of the star. When the DM density in the core is again sufficiently high, DM annihilation can again become efficient and can again power the star. Depending on the released energy by the DM annihilation and the number of trapped annihilation products, this powering can slow down or even stop nuclear burning.

So, one can see that besides gravitation and nuclear burning, also the annihilation of adiabatically contracted and captured DM can contribute the luminosity of the star temporarily. In the following, we describe the particular luminosity contributions.

If the star is in thermal equilibrium, the amount of energy generated in the star is balanced by the transport of that energy towards the surface in order to be radiated away. So,

$$L_\star = L_{tot} \tag{2.4}$$

must be fulfilled. $L_\star$ is the luminosity radiated away from the surface of the star. Here, one assumes black body radiation which leads to a flux of $\sigma_B \, T_{eff}^4$ where

$$\sigma_B = \frac{2\pi^5 k_b^4}{15 h^3 c^2} \tag{2.5}$$

is the Stefan-Boltzmann constant and T_{eff} is the surface temperature of the star. If one integrates this flux over the surface of the sphere at which the radiation of the star is radiated away which has the radius $R_\star$, the so-called photospheric radius, one obtains

$$L_\star = 4\pi R_\star^2 \sigma_B T_{eff}^4. \tag{2.6}$$

L_{tot} in equation 2.4 is the total luminosity of the DS

$$L_{tot} = L_\chi + L_{grav} + L_{nuc} + L_C, \tag{2.7}$$

which consists of the luminosity contributions for the contracted DM L_χ, gravitation L_{grav}, nuclear fusion L_{nuc}, and captured DM L_C.

The various contributions are explained in the following.

Annihilation of adiabatically contracted DM

The first contribution to the luminosity comes from the annihilation of adiabatically contracted DM which is important during the protostellar phase. This contribution takes the form

$$L_\chi = 2 m_\chi \, f_Q \, \Gamma_A. \tag{2.8}$$

It depends on twice the DM mass m_χ, since there are always two DM particles annihilating, the fraction of annihilation energy that is transfered to particles which are trapped inside the star f_Q, and the annihilation rate Γ_A. The annihilation rate can be expressed by

$$\Gamma_A = \int d^3r\, n_\chi(r)^2 \; < \sigma v >_{ann} \tag{2.9}$$

where $n_\chi(r)$ is the number density of the DM particles in the star at distance r and $< \sigma v >_{ann}$ is the annihilation cross section. Putting equations 2.8 and 2.9 together, and changing $n_\chi(r)$ to the DM mass density inside the star $\rho_\chi(r)$, the final expression for the luminosity contribution coming from annihilation of contracted DM can be written as

$$L_\chi = \frac{2}{m_\chi} f_Q \int d^3r\, \rho_\chi(r)^2 \; < \sigma v >_{ann} . \tag{2.10}$$

Gravitational contraction

After the DM fuel runs out, the star continues contraction in order to maintain the photon pressure. At this time, the DS phase is over and gravitation briefly powers the star.

To obtain the formula for the gravitational contribution, one needs the potential energy of the star per shell

$$dE_{grav} = -\frac{G\, M(r)}{r}\, dm \tag{2.11}$$

where $M(r)$ is the enclosed mass at radius r and dm is the mass inside a shell. This can be written as $dm = 4\pi r^2\, \rho(r) dr$ where $\rho(r)$ is the nucleon denisty at radius r. Now we can use the virial theorem

$$-\frac{1}{2} E_{grav} = E_{rad}. \tag{2.12}$$

The virial theorem states that the kinetic energy in the star is minus half of the potential energy. If the star shrinks, the gravitational potential rises but the kinetic energy in the star will only compensate for half of this rise in the form of heating. The other half will be radiated away. This process is important during the inital contraction of the molecular cloud to a protostar.

The contribution to the total luminosity coming from gravitational contraction is

$$L_{grav} = -\frac{1}{2}\frac{d}{dt} E_{grav}. \tag{2.13}$$

Nuclear fusion

When the star contracts, the temperature in the star increases. If the core reaches a temperature of $\sim 10^7$ K, nuclear fusion begins [28]. An example for a fusion process is the proton-proton-cycle in which hydrogen is converted to helium. It dominates for lower temperatures.

The contribution to L_{tot} coming from nuclear burning can be written as

$$L_{nuc} = \sum_i \int_0^R dr\, 4\pi r^2\, \rho(r)\, \epsilon_i(r) \tag{2.14}$$

where R is the radius of the star, and $\epsilon_i(r)$ is the energy generation at the distance r of the fusion process i. One has to sum over all the fusion processes i to obtain the total nuclear luminosity L_{nuc}.

The energy generation rate of the proton-proton-cycle for example is

$$\epsilon_{pp}(r) \propto \rho(r)\, X(r)^2\, T(r)^4 \tag{2.15}$$

where $X(r)$ is the mass fraction of hydrogen, and $T(r)$ is the temperature, both at distance r.

Annihilation of captured DM

After the annihilation of adiabatically contracted DM, the DS can be refueled via captured DM.

When the star has contracted, it is denser and DM capture becomes more efficient. The captured DM thermalizes and can be described by a Boltzmann distribution ρ_C inside of the star [28]. One has to be careful to not mix up the Boltzmann distribution with the Maxwell-Boltzmann distribution. The Maxwell-Boltzmann distribution describes the velocities of particles in idealized gases which are in thermal equilibrium, whereas the density profile of a gas in thermal equillibrium bound in a gravitational field can be described with the Boltzmann distribution. Both, ρ_χ from above and ρ_C, describe the DM density inside of the star, but at different stellar stages. ρ_χ is the DM density in the star during the protostellar phase where the DM particles accumulate in the center of the star due to adiabatical contraction of DM. This DM fuel already runs out before nuclear fusion has started. ρ_C is the DM density inside the star which is contributed by captured DM.

The contribution L_C first takes the same form as equation 2.8 since the luminosity also comes from DM annihilations. Assuming that DM capture and annihilation are quickly in equilibrium, we can use

$$\Gamma_A = \frac{1}{2} C \tag{2.16}$$

where C is the DM capture rate. This relation for the equilibrium between the DM capture rate and annihilation is derived in appendix C. Using equations 2.8 and 2.16, and renaming the luminosity contribution to L_C in order to visualize the difference between the two stages of DM annihilation, we can write

$$L_C = f_Q\, m_\chi\, C. \tag{2.17}$$

Equation 2.17 shows that DM capture can contribute to the total luminosity of the star.

2.2.3. Dark matter fueled stars as solution for the paradox of youth

The region near the galactic center contains $\sim$ 200 young, massive stars [29] which is very surprising. Their age was determined by spectroscopy and it turned out that these stars were formed during a time, when the black hole in the galactic center has already existed. But with a black hole in the center of the galaxy, the formation of stars in the immediate vicinity of the center is unlikely due to the strong tidal forces of the black hole. These forces occur since the gravitational force is not the same over the entire object. While the part of a molecular cloud or a new forming star close to the black hole feels a strong gravitational pull, the part further away feels a less strong gravitational pull. As a consequence of that, the object is pulled apart. The fact that there are still stars which were apparently formed in this hostile environment is called the "paradox of youth" [29].

One explanation for the paradox of youth could be e.g. star migration [30]. In this scenario, stars were produced in a less hostile environment and migrated towards the galactic center via a gravitational drag triggered by gravitational interactions with the surrounding matter, called "dynamical friction". This leads to a loss in kinetic energy and momentum.

Another explanation is based on the idea that we described in the previous subsection. Here, they would be stars which are temporarily powered by DM annihilation of captured DM. If the nuclear fusion was sufficiently slowed down, or stopped for a certain time, the star in reality was formed earlier than expected, maybe even in a time before this region was such a hostile environment.

These young stars close to the center of the galaxy to which the paradox of youth applies are classified by their mass, radius and temperature to be O-B-stars [31]. We explain the meaning of the prefix "O-B" in appendix A in more detail. O-B-stars can reach very high rotation velocities [32], which are close to the break-up velocity of the star. Since the rotation velocity can be very high in this case, considering the rotation of these stars could have a strong influence on the DM capture rate. This was one motivation for this work.

2.2.4. Detectability of Dark Stars

A possible way to detect DSs is determining the luminosity and surface temperature. As one can see in figure 2.4, the main sequence shifts to lower temperatures and higher luminosities for DSs. The deviation from the ordinary main sequence becomes larger, the higher the local DM halo density is since then, DM capture and therefore also DM annihilation is more efficient.

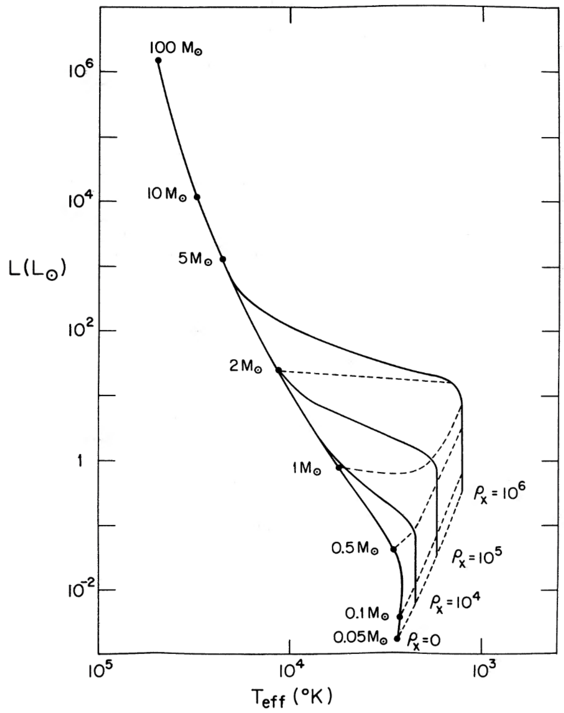

Figure 2.4.: Main sequence for stars with different ambient DM densities. Ambient DM density given in units of $\frac{M_\odot}{pc^3} = 38\,\frac{GeV}{cm^3}$. The figure was taken from [33].

One can also see in figure 2.4 that the effect is larger for smaller masses of the star. So O-B-stars seem to be a bad object to study the influence of DM capture on the stellar evolution, but it is still interesting to check if the rotation might increase the capture strongly such that the influence of DM on the stellar evolution becomes larger than expected due to previous analyses.

2.3. IceCube

As mentioned in the introduction, besides direct detection experiments and astrophysical effects, indirect detection is a promising way to confirm the existence of DM. Most indirect detection approaches are based on the trapping of DM particles in deep gravitational wells of heavy stellar objects and the annihilation of DM to Standard Model (SM) particles. Whereas charged particles and photons are mostly trapped inside the star and affect its evolution, neutrinos can escape and can be seen by detectors on earth. After a certain time, an equilibrium between capture and annihilation in the star sets in which leads to a constant flux of neutrinos moving towards the earth. These neutrinos are directional and have a different energy spectrum than the atmospheric neutrino background. The region in the sun where the majority of these annihilations take place is the center, which is very small. So this can be compared to a search for a pointlike neutrino source. The expected signal is lying in between a few GeV and

$\sim$ 1 TeV. Higher energetic neutrinos have an interaction length that is significantly smaller than the radius of the sun, so they are mostly trapped inside the sun [17]. One experiment examining this process is IceCube [17, 34]

2.3.1. The detector

IceCube is a neutrino detector with a size of one cubic kilometer [17], located in the ice [35] at the geographic South Pole, Antarctica. It is installed between the depths 1450 m and 2450 m. Construction was started in 2005 and it is running since May 2011 [17].

The neutrinos are reconstructed by optical detection of Cherenkov radiation. The Cherenkov radiation is caused by secondary particles produced by neutrino interactions in the ice or the nearby bedrock. These photons are detected by photomultiplier tubes (PMT) [36] placed in Digital Optical Modules (DOM) [37].

The IceCube installation consists of 78 strings ordered in a hexagonal grid with about 125m between each string. Each of these strings provides 60 DOMs spaced by 17m along the string. There, energies of $\sim$ 100 GeV can be detected [17].

DeepCore completes the set-up. It consists of 8 additional strings with a reduced DOM spacing of 7 m and higher quantum efficiency multiplier tubes. They are optimized to detect neutrinos at lower energies down to $\sim$ 10 GeV [17]. DeepCore is located near the central string of IceCube and mostly below a layer of dust at depths between 1860 m and 2100 m [17, 34]. The DeepCore strings are completed by 10 more DOMs above the dust layer, functioning as veto cap [34]. In addition to the PMT, a DOM also contains an electronics board. With that, the signals are digitized and get a time stamp. After transmission of the information to the surface, the signals of all PMTs are evaluated. The time stamps shed light onto the direction and by investigating the PMT counts, the energy can be estimated [38]. In figure 2.5, the whole IceCube array is shown.

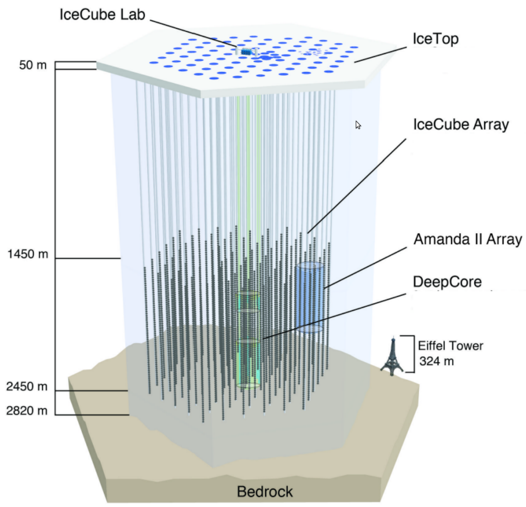

Figure 2.5.: Array of the IceCube observatory, picture taken from [38]

2.3.2. Methods to identify neutrinos

The reason why IceCube was built deep inside the ice is shielding the background. However, due to its size, a background of atmospheric cosmic-ray muons is still detected at a rate of 3000 per second [38]. So it is important to find reliable methods to identify neutrinos. In [38], two methods are presented.

The first method focuses on so-called track events where muon neutrinos interact mainly outside the detector producing long muon tracks traversing the IceCube array. An advantage of this method is an angular resolution of $\leq 0.4°$ that allows to point back the long tracks to the source. Another advantage is that one can detect neutrinos that interacted outside of the detector. However, a disadvantage is the huge background of cosmic-ray muons. An idea that solves this problem is using the earth as filter in order to remove background. Thereby, one distinguishes between up- and downgoing events. Downgoing events are events triggered by neutrinos coming directly from the sky above, whereas upgoing events are triggered by neutrinos that travelled through the earth before entering the detector from underneath. By only taking upgoing events into account, one can exclude that one has a background of cosmic-ray muons since they are filtered out by the earth. So, limits from this method do not come only from the fact that only one single flavor can be viewed. As a result of using the earth as a filter, only half of the sky can be observed.

The second method is used for cascade events to identify e.g. high-energy neutrinos interacting inside the detector, the so-called high-energy starting events (HESE). For HESE, the IceCube volume is divided into an outer veto shield and an inner fiducial volume. In this case, only events inside the detector can be detected, but the detector serves as total absorption calorimeter that measures neutrino energy cascades with a 10 - 15 % resolution

[39]. Additional advantages are that the observation covers the whole sky, and that both, muon tracks and secondary showers of charged current (CC) interactions of electron and tau neutrinos and neutral current (NC) interactions of neutrinos of all flavors can be detected. A disadvantage is that the direction reconstruction is still in development. The resolution is $10° \sim 15°$ [39]. This is the reason for not using the earth as a filter, because the directional resolution is too bad to distinguish between up- and downgoing events.

In figure 2.6 we can see the Cherenkov pattern of an electron/tau neutrino track with ≈ 1 PeV and a muon neutrino track with 2.6 PeV.

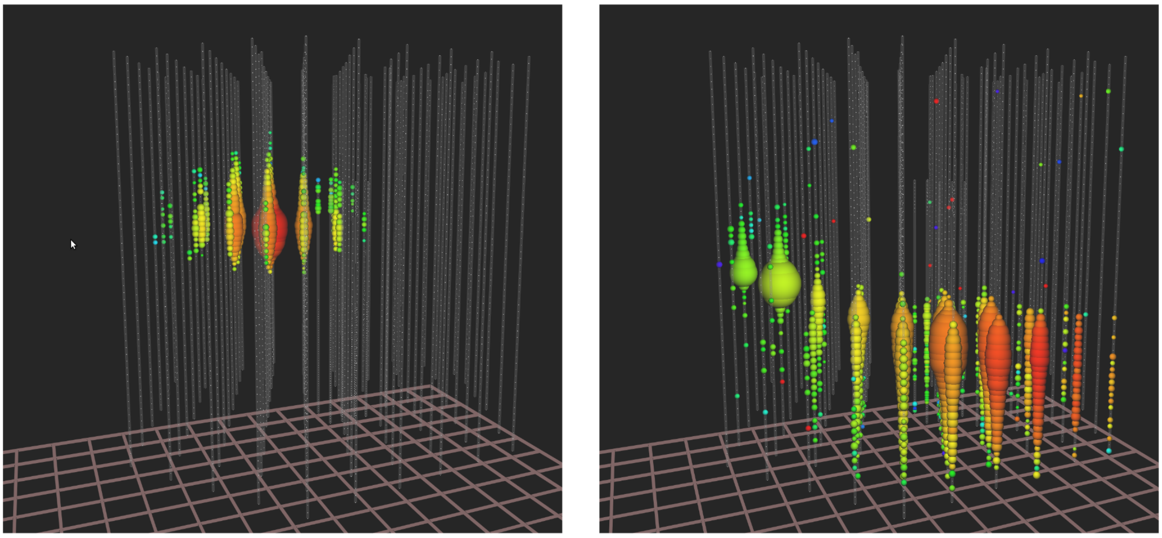

Figure 2.6.: Left picture: Result of a shower in IceCube triggered by an electron or tau neutrino. The measured energy was ≈ 1 PeV.
Right picture: Result for an upgoing muon track. The measured energy was 2.6 PeV.
The white dots represent sensors without signal. The color of the other dots indicate the arrival time. Red means early arrival and purple means late arrival, following the rainbow colors. The size of the points makes it possible to deduce the amount of photons.
The picture was taken from [38].

2.3.3. Status of detection

So far, there was no significant excess of events that exceeded the background for neutrinos coming from the annihilation of DM particles inside the sun. But it allows to set limits on an exotic flux component coming from the sun. This can be translated to a limit on the WIMP-proton scattering cross section by assuming a local DM halo density of $0.3\,\frac{GeV}{cm^3}$, a Maxwell-Boltzmann distribution as velocity distribution for the halo DM particles, the Standard Solar Model and a given annhilation channel.

For the spin-dependent (SD) scattering cross section IceCube provides constraints competitive with those from direct detection experiments in the region above ~ 80 GeV [17] as it can be seen in figure 2.7.

In figure 2.7, and also in figure 2.8, they use three different channels, two 'hard' channels where the DM particles decay into W^+W^- and $\tau^+\tau^-$, and one 'soft' channel $b\bar{b}$. The W bosons and τ's promptly decay and the energy of the produced neutrinos peaks close to the DM mass. These are the decay channels, the neutrinos obtain the most energy. In this case, many neutrinos exceed the energy threshold of IceCube and one obtains better limits. The opposite is the case for the 'soft' channel $b\bar{b}$. In this decay, the neutrinos obtain relatively little energy, only a small amount of neutrinos exceed the IceCube threshold and one obtains the worst limit.

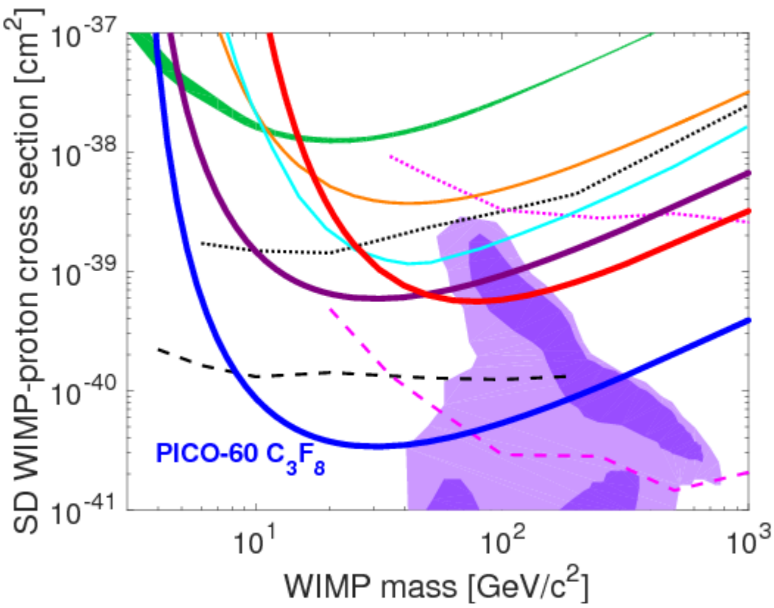

Figure 2.7.: Limits on the spin-dependent scattering cross section, $\sigma^{SD}_{\chi-p}$, obtained from PICO-60 C_3F_8 (thick blue) [16], PICO-60 CF_3I (thick red) [40], PICO-2L (thick purple) [41], PICASSO (green band) [42], SIMPLE (orange) [43], PandaX-II (cyan) [44], IceCube (dashed and dotted pink) [17], and SuperK (dashed and dotted black) [21, 22]. The limits from IceCube and SuperK assume the annihilation channels $\tau^+\tau^-$ (dashed) and $b\bar{b}$ (dotted). The figure was taken from [16].

For the spin-independent (SI) scattering cross section, the results of IceCube and direct detection experiments complement one another, as shown in figure 2.8. Since the IceCube results underlie uncertainties from the nuclear scattering process and astrophysics, they only seem to be significantly stronger with respect to the other limits. However, they have improved by a factor of $\sim$ 2 to 4 [17] compared to other neutrino telescope limits [34, 45].

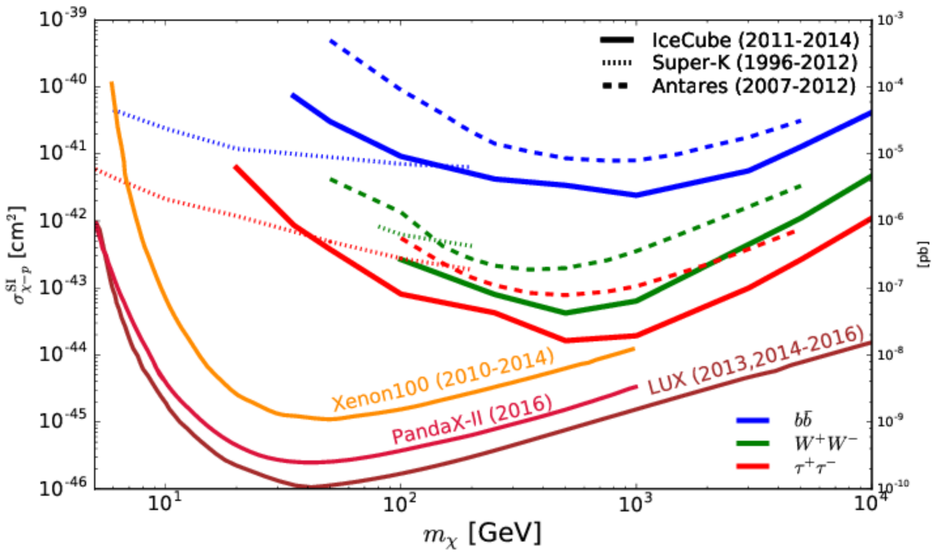

Figure 2.8.: Limits on the spin-independent scattering cross section, $\sigma^{SI}_{\chi-p}$, for three different channels ($b\bar{b}$, W^+W^-, $\tau^+\tau^-$), compared to results of other neutrino detectors and direct detection experiments [46, 47, 48, 49, 50]. Systematic uncertainties included in IceCube limits. The figure was taken from [17].

Although the SI limits from IceCube are much weaker than those obtained from direct detection experiments, they are nevertheless interesting, because they have other particle and astrophysical uncertainties than the SD limits.

2.4. Summary of the chapter 'Basics'

DM presents a solution for several inconsistencies on different scales, e.g. in the CMB anisotropies or in the rotation curves of galaxies. In addition to direct detection experiments, which are not discussed in this work, there is also indirect detection and observation of astrophysical effects due to DM capture and annihilation in stars. In the latter case we could see the effect that some stars look younger than they actually are. While star processes such as nuclear fusion cause the star to age, the supply of energy through DM annihilation products can cause a slowdown in the aging process. Another indication for DM annihilations would be a neutrino flux coming from the sun with a certain energy spectrum. It is one of IceCube's tasks to detect this flux. Even if the flux is not detected, IceCube can set stronger constraints on the WIMP-proton scattering cross section. All this is based on DM annihilations which is in turn connected with DM capture. In order to make realistic predictions, it is essential to have a description of the DM capture rate as exact as possible. So far, the rotation of the star was not considered. To see if the consideration of the rotation has significant influence on the DM capture rate was the main goal of this thesis. In the next chapter, we present the formula for the capture rate how it was used so far. Furthermore, we explain how the rotation comes in, and which form the modified formula takes then.

3. Dark matter capture

As seen in chapter 2, DM capture can have a strong influence on the formation and evolution of stars and particle physics, and as mentioned before, the rotation of stars was neglected so far. In this chapter, we step by step reformulate the expression for the DM capture rate by considering the rotation of stars to see whether this has a significant impact on the DM capture rate. In the following sections, we use many different variables and indices. For an overview of them, see appendix B.

3.1. The dark matter capture rate for a non-rotating star

The formalism for the DM capture rate in celestial bodies was presented in a paper by Gould in 1987. In the following, we derive the formula for the capture rate of DM particles in non-rotating stars analogous to [23].

At the beginning, we consider a spherical shell with radius r and thickness dr which is located in a spherically symmetric gravitational field. The escape velocity at the shell is $u_{esc}(r)$. $\Omega^{-}_{u_{esc}}(w)$ is defined as rate per unit time that a DM particle with an initial velocity w scatters down to a velocity less than $u_{esc}(r)$ while travelling through the shell.

In the next step, we imagine a surface with radius R, where R is so large that the gravitational field at R is negligible. In order to get an expression for the flux of DM particles through the surface, we need the velocity distribution which is infinitely far away from the star where the gravitational field is negligible, $f(u)\,du$. He used $u = |\ \vec{u}\ |$, because of the assumption that the velocity distribution is isotropic. If the velocity distribution is isotropic, we can write

$$f(u)\,du \;\rightarrow\; \frac{1}{2}\,f(u)\,du\,d\cos\,\theta \tag{3.1}$$

where θ is the angle relative to the radial direction, and the velocity of the DM particles perpendicular to the surface is u cos θ. Using this, we can write the DM flux traversing the surface as

$$F_\chi \;=\; \frac{1}{2}\,f(u)\,u\,\cos\,\theta\,du\,d\cos\,\theta \tag{3.2}$$

After changing the integrand in 3.2 from $d\cos\,\theta$ to $d\cos^2\theta$, the expression for the flux finally writes as

$$F_\chi \;=\; \frac{1}{4}\,f(u)\,u\,du\,d\cos^2\theta \qquad 0 \,\leq\, \theta \,<\, \frac{\pi}{2}. \tag{3.3}$$

The interval $\frac{\pi}{2} \leq \theta \leq \pi$ is not considered since the DM particles moving under this angle do not fly through the surface.

Now, we change the variable $d\cos^2\theta$ to the angular momentum per unit mass

$$J = R\,u\,\sin\theta \qquad d\cos^2\theta = \frac{d\,J^2}{R^2\,u^2}, \tag{3.4}$$

which becomes important later. After summing over all the area elements, we get the expression for the rate of incoming DM particles in a $d\,J^2$ interval

$$R_\chi = 4\,\pi\,R^2\,\frac{1}{4}\,f(u)\,u\,du\,\frac{d\,J^2}{R^2\,u^2}. \tag{3.5}$$

If the velocity of the DM particle at infinity is u, it will be accelerated by the gravitational field from the star, and will have the velocity

$$w^2(r) = u^2 + {u_{esc}}^2(r) \tag{3.6}$$

at the distance r. Here, the escape velocity is the velocity needed to escape from the gravitational potential of the star. For an arbitary enclosed mass profile $M(r)$ in the star it is defined as

$$u_{esc}(r) = \sqrt{\frac{2}{m_\chi}\int_r^\infty \frac{GM(r')m_\chi}{r'^2}\,dr'} \tag{3.7}$$

To capture a DM particle, the initial velocity $w(r)$ must be decreased by scattering to a velocity smaller than $u_{esc}(r)$. The probability that this happens is

$$p(w \rightarrow w' < u_{esc}) = \Omega^-_{u_{esc}}(w)\,\frac{dl}{w} \tag{3.8}$$

where $\Omega^-_{u_{esc}}(w)$ indicates the rate per unit time that a DM particle with an initial velocity w scatters down to a velocity less than $u_{esc}(r)$ while travelling through the shell, as mentioned above, and $\frac{dl}{w}$ describes the differential time required for the DM particles to travers the shell.

To determine $\Omega^-_{u_{esc}}(w)$, we first investigate the differential cross section $\frac{d\sigma}{dQ}$ of the scattering between the incoming DM particle and the nucleon inside the star. If the target is at rest before the scattering, the kinematic limits for the energy transfer Q are given by

$$Q_{minimal} = 0 \tag{3.9}$$

$$Q_{max} = \frac{1}{2}\,m_\chi\,\beta_+\,w^2 \tag{3.10}$$

with

$$\beta_\pm = \frac{4\,m_i\,m_\chi}{(m_i \pm m_\chi)^2}. \tag{3.11}$$

Here, m_χ denotes the mass of the DM particle and m_i is the mass of nucleon i. These limits are obtained by momentum and energy conservation. Within this range all energy transfers have the same probability. If the total cross section is denoted as σ_{tot}, the differential cross section can be written as

$$\frac{d\sigma}{dQ} = \frac{1}{Q_{max}}\,\sigma_{tot}\,\Theta\,(Q_{max} - Q). \tag{3.12}$$

To be captured, a WIMP has to lose enough energy, so that its velocity is below $u_{esc}(r)$ after the scattering. From this the minimal required energy transfer can be determined to be

$$Q_{min} = \frac{1}{2}\,m_\chi\,u^2. \tag{3.13}$$

With the differential cross section and the minimal energy transfer needed for a WIMP to be captured we can define the downscattering rate $\Omega^-_{u_{esc}}(w)$ to be

$$\Omega^-_{u_{esc}}(w) = n_i(r)\,w\int_{Q_{min}}^{Q_{maximal}}\frac{d\sigma}{dQ}\,dQ = \sigma_{tot}\,n_i(r)\,w\,\frac{Q_{max} - Q_{min}}{Q_{max}}\,\Theta\,(Q_{max} - Q_{min}) \tag{3.14}$$

This equation gives the total rate of scattering, $\sigma_{tot}\,n_i(r)\,w$, multiplied by the probability that a scattered DM particle has lost enough energy to be captured after the scattering. Here, σ_{tot} is the total cross section and $n_i(r)$ is the number denisty of the nucleon i at the distance r to the center of the star.
So the first part of equation 3.8 is derived.

The second part of equation 3.8, $dt = \frac{dl}{w}$, is the differential time which the DM particle needs to travel through the shell. The relation

$$dl = \frac{dr}{cos\,\theta} \tag{3.15}$$

applies, where dl is the differential distance covered by the DM particle in the shell. With $J = rw\,\sin\theta$ we can write

$$dl = \frac{dr}{\sqrt{1 - \frac{J^2}{r^2\,w^2}}}. \tag{3.16}$$

Using $dr = \frac{dJ}{w\sin\theta}$, we can rewrite equation 3.16 and we obtain the differential time

$$dt = \frac{1}{w}\left(1 - \frac{J^2}{r^2\,w^2}\right)^{-\frac{1}{2}}\,dJ \times 2\,\Theta\,(r\,w - J) \tag{3.17}$$

where the Heaviside function and an additional factor was added. Here, the angular momentum per unit mass becomes important in the Heaviside function. It causes the DM particle to move only through the shell if the angular momentum is small enough, namely $rw < J$, to reach r. The 2 comes from the fact that if the DM particle moves through the shell, it would move through dl always twice.

By multiplying now 3.5 and 3.8, plugging in 3.17 and integrating over all angular momenta, we obtain the number of DM particles per unit time, unit velocity and unit volume. The DM capture rate can then be written as the integral over the volume of the star and over the velocity distribution.

$$C = \sum_i \frac{\rho_H}{m_\chi} \int dV \int du \, \frac{f(u)}{u} \, w \, \Omega^-_{u_{esc}}(w) \tag{3.18}$$

where ρ_H is the local dark matter halo density, usually set to $0.3 \, \frac{GeV}{cm^3}$ [51]. To get the total capture rate, all contributions of every element in the star have to be added up. For this reason, the sum over i was added to equation 3.18.

It is important to note that for large energy transfers a form factor has to be added. In [23], Gould used the Helm form factor

$$\mid F(q^2) \mid^2 = \exp\left(-\frac{q^2 R_i^2}{3\hbar^2}\right) \tag{3.19}$$

where q is the momentum transfer, R_i is the radius of nucleon i and $c = 1$. In the following calculations we assume for simplicity that $\mid F(q^2) \mid^2 = 1$.

This is the capture formalism used since the 80s. In the following sections, we present two approaches where rotation is considered.

3.2. The dark matter capture rate for a rotating star

The following sections contain the improvements for the capture rate. We fully perform the first approach, later called SRF approach, in the SRF. For the second approach, we use the advantages that the probabilities for all possible recoil energies are the same in the TRF, and that the escape velocity takes a simple form in the SRF. This approach we later call 'hybrid approach' since it combines the advantages of both, the SRF and TRF. But first of all, we explain the choice of the reference frames in more detail.

3.2.1. Comparison between the different frames

Trivially, the standard choice of the reference frame is actually the frame in which the target is at rest (TRF). One reason for this is that one can set the initial velocity of the target particle equal to zero, which may simplify the calculation. Another reason is that the cross section is well known. So, for a non-rotating star, meaning that the target particles have no velocity before the scattering, the choice of the reference frame is clear. One chooses the TRF, which simultaneously corresponds to the rest frame of the star (SRF) in the case of the non-moving target particles.

For a rotating star, however, the question arises as to whether the TRF is the most suitable reference frame. An advantage of the TRF is still the cross section which is well known. One challenge, however, is determining the escape velocity. Since the gravitational field is no longer isotropic in the TRF as the star rotates, the escape velocity becomes directional in the TRF. To visualize this fact, one can do a thought experiment, which is probably easier to do with the aid of figure 3.1.

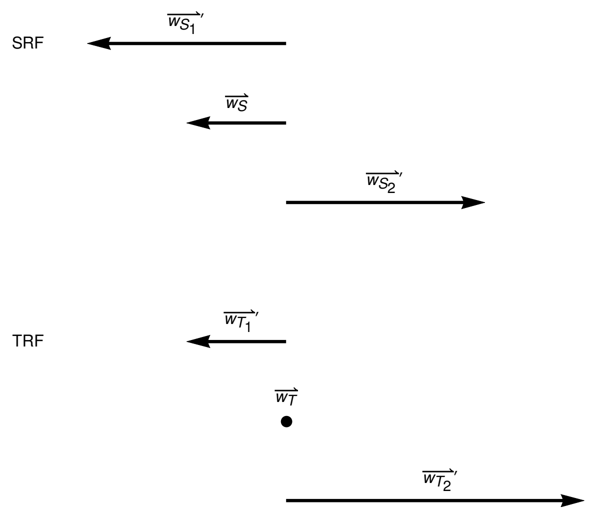

Figure 3.1.: An example for velocities of DM and target particles in the star rest frame (upper part) and in the target rest frame (lower part)

Let us first consider the SRF. Suppose that the escape velocity in the SRF is 7. The target particle moves with velocity 5, which is simultaneously the velocity of the SRF. After collision with the target particle, DM particle No. 1 moves with velocity 10 in the same direction as the target particle and DM particle No. 2 moves with velocity 10 in the opposite direction. Since the modulus of the DM particle velocity is larger than the escape velocity, both DM particles would escape from the star.

After transferring to the TRF, the targets have velocity 0, DM particle No. 1 moves with 5 and DM particle No. 2 moves with 15 (both again in the opposite direction). If the escape velocity remained unchanged, DM particle No. 2 would escape from the star in the TRF, whereas DM particle No. 1 would not. This is in contradiction to the SRF. This very simple example shows that we have to be careful with the expression for the escape velocity in the TRF and that the direction of the incoming and outgoing DM particles play a role for the respective particle. How the escape velocity for the DM particles looks like in the TRF can be seen in the appendix F.

But going from the TRF to the SRF, where the escape velocity is not directional, does not make things necessarily easier, since one has to redetermine the cross section for the SRF. That is why, no matter which way one takes, one has to deal with different challenges in both frames, the SRF and TRF.

In addition to the SRF and TRF, there are also the galactic rest frame (GRF) and the center of mass (COM) frame. In these frames, many problems would occur. In both frames, we neither have the advantage that the target particles are initially at rest, nor that the escape velocity is isotropic. Since the target particles are not at rest initially, we furthermore have to redetermine the cross section in these frames as well.

These are the reasons, why we forgot about the GRF and the COM frame, but there was still the question, which frame to use, SRF or TRF, and how to deal with the particular challenge. We have finally chosen the SRF, since one very quickly loses intuition in the TRF because of the direction dependent escape velocity, so we focussed on the SRF.

It is always good to have the chance to cross check one's results, so we used two different approaches to calculate the dark matter capture rate. We present these two approaches in the following sections.

3.2.2. Derivation of the SRF approach

In this subsection, we finally derive the SRF approach. First, we rewrite the velocity distribution function, in a further step, we determine the kinematic limits for the energy transfer, and finally, we build the formula for the DM capture rate. Important to note is that this approach is only valid if all energy transfers have the same probability as in the case of the target particle at rest.

Derivation of the velocity distribution function

We assume that the DM particles in the galactic halo follow a Maxwell-Boltzmann distribution (MBD). This coincides with the calculated velocity distribution for the earth vicinity by using the empirically obtained NFW density profile. For a comparison between the velocity distribution functions (VDFs), see appendix D. The VDF for the DM particles in the GRF infinitely far away from the star with the velocity $\vec{u}_G$ has the form

$$f(\vec{u}_G) = \left(\frac{1}{\pi\, {v_0}^2}\right)^{\frac{3}{2}} \, e^{-\frac{\vec{u}_G^{\,2}}{{v_0}^2}} . \tag{3.20}$$

Expressed by the velocity of the DM particles infinitely far away from the star in the SRF, the velocity of the DM particle in the GRF $\vec{u}_G$ can be written as $\vec{u}_G = \vec{u}_S + \vec{v}_s$ with

$$\vec{u}_S = \begin{pmatrix} u_S \sin\theta_u \cos\varphi_u \\ u_S \sin\theta_u \sin\varphi_u \\ u_S \cos\theta_u \end{pmatrix} \tag{3.21}$$

and

$$\vec{v}_s = \begin{pmatrix} v_s \sin\alpha \\ 0 \\ v_s \cos\alpha \end{pmatrix}, \tag{3.22}$$

where $\vec{v}_s$ is the velocity of the star motion around the galactic centre which lies in the x-z plane, α is the angle between $\vec{v}_s$ and the angular velocity ω which lies along the z-axis, θ_u is the polar angle and φ_u the azimuth angle of $\vec{u}_S$, which is pictured in figure 3.2. There one can also see $\vec{v}_S$ and φ, where $\vec{v}_S$ is the velocity of the nuclei in the star, lying in the x-y plane and φ is the azimuth angle of $\vec{v}_S$.

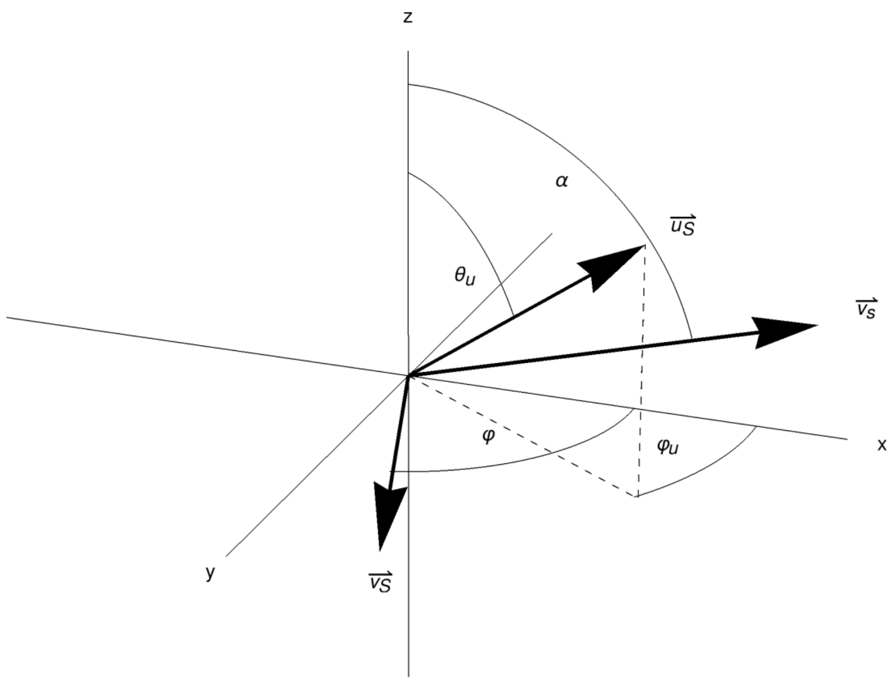

Figure 3.2.: Pictorial representation of $\vec{u}_S$, $\vec{v}_s$, $\vec{v}_S$, α, θ_u, φ_u and φ

The modulus of the velocity of the DM particle has the form

$$\mid \vec{u}_G \mid = \sqrt{u_S^2 + {v_s}^2 + 2\, u_S\, v_s\, (\sin\theta_{u_S}\, \cos\varphi_{u_S}\, \sin\alpha + \cos\theta_{u_S}\, \cos\alpha)}. \tag{3.23}$$

By plugging in equation 3.23 in 3.20, we obtain the expression

$$f(\vec{u}_S, \alpha) = \left(\frac{1}{\pi\, {v_0}^2}\right)^{\frac{3}{2}} \cdot e^{-\frac{u_S^2 + {v_s}^2 + 2\, u_S\, v_s\, (\sin\theta_{u_S}\, \cos\varphi_{u_S}\, \sin\alpha + \cos\theta_{u_S}\, \cos\alpha)}{{v_0}^2}}. \tag{3.24}$$

The probability for $\vec{u}_S$ being in d^3u_S is $f(\vec{u}_S, \alpha)\, u_S^2 \sin\theta_u\, du_S\, d\varphi_u\, d\theta_u$, by using spherical coordinates. The final expression for the VDF which can be used in equation 3.18 is

$$f(\vec{u}_S, \alpha) \;=\; f(u_S, \theta_u, \varphi_u, \alpha). \tag{3.25}$$

Kinematic limits for the energy transfer

In this part, we derive the maximal energy transfer, Q_{max}, and the minimal energy transfer, $Q_{minimal}$, between the DM and target particle.

To determine Q_{max} and $Q_{minimal}$, we use the four equations which we obtain from momentum and energy conservation

$$eq_x \;=\; p_{i_x} \;+\; p_{\chi_x} \;-\; q_{i_x} \;-\; q_{\chi_x} \tag{3.26}$$

$$eq_y \;=\; p_{i_y} \;+\; p_{\chi_y} \;-\; q_{i_y} \;-\; q_{\chi_y} \tag{3.27}$$

$$eq_z \;=\; p_{i_z} \;+\; p_{\chi_z} \;-\; q_{i_z} \;-\; q_{\chi_z} \tag{3.28}$$

$$\begin{aligned} eq_E \;=& \frac{{p_{i_x}}^2 \,+\, {p_{i_y}}^2 \,+\, {p_{i_z}}^2}{2\,m_i} + \frac{{p_{\chi_x}}^2 \,+\, {p_{\chi_y}}^2 \,+\, {p_{\chi_z}}^2}{2\,m_\chi} \\ &- \frac{{q_{i_x}}^2 \,+\, {q_{i_y}}^2 \,+\, {q_{i_z}}^2}{2\,m_i} - \frac{{q_{\chi_x}}^2 \,+\, {q_{\chi_y}}^2 \,+\, {q_{\chi_z}}^2}{2\,m_\chi}, \end{aligned} \tag{3.29}$$

where p denotes the momentum before and q after the scattering. The indices i and χ stand for nucleon i and DM particle, respectively.

To optimize the kinetic energy of the recoiling nucleus, we use the Lagrangian

$$L \;=\; \frac{{q_{i_x}}^2 + {q_{i_y}}^2 + {q_{i_z}}^2}{2\,m_i} \;-\; \lambda_x\, eq_x \;-\; \lambda_y\, eq_y \;-\; \lambda_z eq_z - \lambda_E\, eq_E \tag{3.30}$$

with the Lagrangian multipliers λ_x, λ_y, λ_z and λ_E and the equations of momentum and energy conservation 3.26 to 3.29 as constraints. The next step is to differentiate equation 3.30 with respect to q_{i_x}, q_{i_y}, q_{i_z}, q_{χ_x},q_{χ_y}, q_{χ_z}, λ_x, λ_y, λ_z and λ_E. This leads to a system of equations which can be solved. By plugging in the solutions in the formula for the maximal [minimal] recoil energy

$$Q_{max\,[minimal]} \;=\; \frac{({q_{i_x}}^2 + {q_{i_y}}^2 + {q_{i_z}}^2)_{max\,[minimal]}}{2\,m_i} \;-\; \frac{{p_{i_x}}^2 + {p_{i_y}}^2 + {p_{i_z}}^2}{2\,m_i}, \tag{3.31}$$

we obtain the expression

$$
\begin{aligned}
Q_{max\,[minimal]} = & \frac{1}{2\,m_i\,(m_i\,+\,m_\chi)^2}\,((m_i{}^2\,+\,m_\chi{}^2)\,p_i{}^2\,+\,2\,m_i{}^2\,p_\chi{}^2 \\
& +\,2\,m_i\,(m_i\,-\,m_\chi)\,p_i\,p_\chi\,\cos\varphi_{coll} \\
& +\,[-]\,2\,m_i\,\sqrt{p_i{}^2\,+\,p_\chi{}^2\,+\,2\,p_i\,p_\chi\,\cos\varphi_{coll}} \\
& \cdot\sqrt{m_\chi{}^2\,p_i{}^2\,+\,m_i{}^2\,p_\chi{}^2\,-\,2\,m_i\,m_\chi\,p_i\,p_\chi\,\cos\varphi_{coll}}), \qquad (3.32)
\end{aligned}
$$

where the colliding angle φ_{coll} is the angle between $\vec{v}_S$ and $\vec{u}_S$. To get φ_{coll}, we use the cosine rule

$$\cos(\varphi_{coll})\,=\,\frac{<\vec{u}_S,\vec{v}_S>}{|\,\vec{u}_S\,|\,|\,\vec{v}_S\,|} \qquad (3.33)$$

with

$$\vec{v}_S\,=\,\begin{pmatrix} v_S\,\sin\theta\,\cos\varphi \\ v_S\,\sin\theta\,\sin\varphi \\ v_S\,\cos\theta \end{pmatrix} \qquad (3.34)$$

and for $\vec{u}$ see 3.21. The polar angle θ is equal to $\frac{\pi}{2}$, because $\vec{v}_S$ lies in the x-y plane. The colliding angle φ_{coll} can then be written as

$$\varphi_{coll}\,=\,\cos^{-1}(\sin\theta_u\,\cos(\varphi_u\,-\,\varphi)). \qquad (3.35)$$

We make the following substitutions in equation 3.32 by assuming that the star rotates like a rigid body

$$p_i\,=\,m_i\,\rho\,\omega, \qquad (3.36)$$

where ρ is the smallest distance between the position of the nucleon in the star and the rotation axis and ω is the angular velocity of the star,
and

$$p_\chi\,=\,m_\chi\,w\,=\,m_\chi\,\sqrt{u_S^2\,+\,u_{escS}\,(r)^2}. \qquad (3.37)$$

So we obtain the final expression for the maximal recoil energy

$$
\begin{aligned}
Q_{max} =& \frac{1}{2\, m_i\, (m_i\, +\, m_\chi)^2}\, ((m_i{}^2\, +\, m_\chi{}^2)\, (m_i\, \rho\, \omega)^2\, +\, 2\, m_i{}^2\, (m_\chi\, \sqrt{u_S^2\, +\, u_{escS}\, (r)^2})^2 \\
&+\, 2\, m_i\, (m_i\, -\, m_\chi)\, m_i\, \rho\, \omega\, m_\chi\, \sqrt{u_S^2\, +\, u_{escS}\, (r)^2}\, \cos \varphi_{coll} \\
&+\, 2\, m_i\, (((m_i\, \rho\, \omega)^2\, +\, (m_\chi\, \sqrt{u_S^2\, +\, u_{escS}\, (r)^2})^2 \\
&+\, 2\, m_i\, \rho\, \omega\, m_\chi\, \sqrt{u_S^2\, +\, u_{escS}\, (r)^2}\, \cos \varphi_{coll})^{\frac{1}{2}} \\
&\cdot\, (m_\chi{}^2\, (m_i\, \rho\, \omega)^2\, +\, m_i{}^2\, (m_\chi\, \sqrt{u_S^2\, +\, u_{escS}\, (r)^2})^2 \\
&-\, 2\, m_i\, m_\chi\, m_i\, \rho\, \omega\, m_\chi\, \sqrt{u_S^2\, +\, u_{escS}\, (r)^2}\, \cos \varphi_{coll})^{\frac{1}{2}}\, -\, \frac{(m_i\, \rho\, \omega)^2}{2\, m_i}.
\end{aligned}
\tag{3.38}
$$

The minimal recoil energy is

$$
\begin{aligned}
Q_{minimal} =& \frac{1}{2\, m_i\, (m_i\, +\, m_\chi)^2}\, ((m_i{}^2\, +\, m_\chi{}^2)\, (m_i\, \rho\, \omega)^2\, +\, 2\, m_i{}^2\, (m_\chi\, \sqrt{u_S^2\, +\, u_{escS}\, (r)^2})^2 \\
&+\, 2\, m_i\, (m_i\, -\, m_\chi)\, m_i\, \rho\, \omega\, m_\chi\, \sqrt{u_S^2\, +\, u_{escS}\, (r)^2}\, \cos \varphi_{coll} \\
&-\, 2\, m_i\, (((m_i\, \rho\, \omega)^2\, +\, (m_\chi\, \sqrt{u_S^2\, +\, u_{escS}\, (r)^2})^2 \\
&+\, 2\, m_i\, \rho\, \omega\, m_\chi\, \sqrt{u_S^2\, +\, u_{escS}\, (r)^2}\, \cos \varphi_{coll})^{\frac{1}{2}} \\
&\cdot\, (m_\chi{}^2\, (m_i\, \rho\, \omega)^2\, +\, m_i{}^2\, (m_\chi\, \sqrt{u_S^2\, +\, u_{escS}\, (r)^2})^2 \\
&-\, 2\, m_i\, m_\chi\, m_i\, \rho\, \omega\, m_\chi\, \sqrt{u_S^2\, +\, u_{escS}\, (r)^2}\, \cos \varphi_{coll})^{\frac{1}{2}}\, -\, \frac{(m_i\, \rho\, \omega)^2}{2\, m_i}.
\end{aligned}
\tag{3.39}
$$

The dark matter capture rate in the SRF approach

Combining the results for the VDF and the kinematic limits, Q_{max} and $Q_{minimal}$, we can build the formula for the DM capture rate.

The downscattering rate $\Omega^-_{u_{esc}}(w)$ can be written as

$$
\Omega^-_{u_{esc}}(w)\, =\, n_i(r)\, \sigma_{tot}\, w_{rel}\, \frac{Q_{max}\, -\, Q_{min}}{Q_{max}\, -\, Q_{minimal}}\, \Theta\, (Q_{max}\, -\, Q_{min}) \tag{3.40}
$$

where $n_i(r)$ is the target density of nucleon i at the distance r to the star center, σ_{tot} is the total cross section and w_{rel} is the relative velocity between the DM and target particles. The numerator $Q_{max} - Q_{min}$ describes the range for the energy transfer where capture is possible and the nominator $Q_{max} - Q_{minimal}$ describes all kinematically possible energy transfers. So the fraction in 3.40 is the probability that a DM particle is captured if it has scattered off a nucleon.

The final formula for the capture is then

$$C = \sum_i \frac{\rho_H}{m_\chi} \int dV \int d^3u_S \, \frac{f(\vec{u}_S, \alpha)}{u_S} \, w_S \, \Omega^-_{u_{esc_S}}(w) \tag{3.41}$$

where we sum over all the different kinds of nuclei i inside the star.

3.2.3. Derivation of the hybrid approach

In this section, we derive the capture formula by using the advantages of both frame, the SRF and TRF. No matter in which frame we work, we have to check in the end whether the velocity of the DM particles after the scattering $|\vec{w}'_S|$ is smaller than the escape velocity at the scattering point. We want to check this in the SRF, using the simple expression for the escape velocity. So the main goal of this section is to derive the expression for the DM velocity after scattering in the SRF, $|\vec{w}'_S|$.

For this, we first go from the SRF to the TRF by shifting the velocities by $-\vec{v}_S$.

$$\vec{w}_T = \vec{w}_S - \vec{v}_S \tag{3.42}$$

$$\vec{v}_T = \vec{v}_S - \vec{v}_S \tag{3.43}$$

The differential cross section is

$$\frac{d\sigma}{dE_{RT}}(|\vec{w}_T|, E_{RT}) = \frac{m_i}{2\,\mu^2\,|\vec{w}_T|^2}\,\sigma_{tot} \tag{3.44}$$

with the recoil energy in the TRF, E_{RT}.
The kinematic limits are

$$E_{RT}^{max} = \frac{2\,\mu^2\,|\vec{w}_T|^2}{m_i} \tag{3.45}$$

$$E_{RT}^{min} = 0. \tag{3.46}$$

The modulus of the velocity of the final-state-particles in the TRF are given by

$$v'_T = |\vec{v}'_T| = \sqrt{\frac{2\,E_{RT}}{m_i}} \tag{3.47}$$

for the target, and

$$w'_T = |\vec{w}'_T| = \sqrt{w_T^2 - \frac{2\,E_{RT}}{m_\chi}} \tag{3.48}$$

for the DM particle.
The angle between the incoming and outgoing particle can be calculated by squaring the

equation for momentum conservation

$$\cos\,\theta_T \;=\; \frac{w_T^2 \,+\, w_T'^2 \,-\, \frac{m_i^2}{m_\chi^2}\, v_T'^2}{2\, w_T\, w_T'}. \tag{3.49}$$

The next step is to rotate the arbitrary velocity vector so that it is parallel to the z-axis.
First, we rotate $\vec{w_T} \;=\; \begin{pmatrix} w_{Tx} \\ w_{Ty} \\ w_{Tz} \end{pmatrix}$ around the z-axis with the rotation matrix
$A_z \;=\; \begin{bmatrix} \cos\,\theta_z & -\sin\,\theta_z & 0 \\ \sin\,\theta_z & \cos\,\theta_z & 0 \\ 0 & 0 & 1 \end{bmatrix}$ so that the vector $\tilde{\vec{v}}_T$ lies in the y-z-plain.
So

$$A_z \,\cdot\, \vec{w}_T \;=\; \begin{pmatrix} 0 \\ \tilde{w}_{Ty} \\ \tilde{w}_{Tz} \end{pmatrix} \tag{3.50}$$

must be fulfilled.
This follows $\cos\,\theta_z\, w_{Tx} \,-\, \sin\,\theta_z\, w_{Ty} \;=\; 0$ and leads to the condition

$$t_{12} \;\equiv\; \tan\,\theta_z \;=\; \frac{w_{Tx}}{w_{Ty}} \tag{3.51}$$

and

$$\tilde{\vec{w}}_T \;=\; \begin{pmatrix} 0 \\ \sin\,\theta_z\, w_{Tx} \,+\, \cos\,\theta_z\, w_{Ty} \\ w_{Tz} \end{pmatrix}. \tag{3.52}$$

The next step is to rotate $\tilde{\vec{w}}_T$ around the x-axis with the rotation matrix
$A_x \;=\; \begin{bmatrix} 1 & 0 & 0 \\ 0 & \cos\,\theta_x & -\,\sin\,\theta_x \\ 0 & \sin\,\theta_x & \cos\,\theta_x \end{bmatrix}$ so that the vector $\vec{w_{Trot}}$ is parallel to the z-axis.
So

$$A_x \,\cdot\, \tilde{\vec{w}}_T \;=\; \begin{pmatrix} 0 \\ 0 \\ w_{\tilde{T}z_{rot}} \end{pmatrix} \tag{3.53}$$

must be fulfilled.
This follows $\cos\,\theta_x\,(\sin\,\theta_z\, w_{Tx} \,+\, \cos\,\theta_z\, w_{Ty}) \,-\, \sin\,\theta_x\, w_{Tz} \;=\; 0$ and leads to the condition

$$t_{23} \;=\; \tan\,\theta_x \;=\; \frac{\sin\,\theta_z\, w_{Tx} \,+\, \cos\,\theta_z\, w_{Ty}}{w_{Tz}}. \tag{3.54}$$

If the polar angle of the incoming DM particle θ_{w_S} is smaller than $\frac{\pi}{2}$, one has to add π to θ_x. Otherwise, the velocity would point in the negative z-direction.

The rotation matrix is then defined by

$$R = A_x \cdot A_z = \begin{bmatrix} 1 & 0 & 0 \\ 0 & c_{23} & -s_{23} \\ 0 & s_{23} & c_{23} \end{bmatrix} \begin{bmatrix} c_{12} & -s_{12} & 0 \\ s_{12} & c_{12} & 0 \\ 0 & 0 & 1 \end{bmatrix} = \begin{bmatrix} c_{12} & -s_{12} & 0 \\ c_{23}\, s_{12} & c_{23}\, c_{12} & -s_{23} \\ s_{23}\, s_{12} & s_{23}\, c_{12} & c_{23} \end{bmatrix}. \tag{3.55}$$

In the rotated TRF the DM particle has the velocity

$$\vec{w}'_{T_{rot}} = |\vec{w}'_T| \begin{pmatrix} \sin\theta_T \sin\phi \\ \sin\theta_T \cos\phi \\ \cos\theta_T \end{pmatrix} \tag{3.56}$$

where ϕ is a free parameter.
To obtain finally $\vec{w}'_T$ we multiplie the inverse of 3.55 with 3.56 and we obtain

$$\vec{w}'_T = \begin{pmatrix} (c_{12}\, s_\varphi + s_{12}\, c_{23}\, c_\varphi) \sin\theta_T + s_{12}\, s_{23} \cos\theta_T \\ (c_{12}\, c_{23}\, c_\varphi - s_{12}\, s_\varphi) \sin\theta_T + c_{12}\, s_{23} \cos\theta_T \\ -s_{23}\, c_\varphi \sin\theta_T + c_{23} \cos\theta_T \end{pmatrix} |\vec{w}_T|. \tag{3.57}$$

The last step is to go back to the SRF

$$\vec{w}_S = \vec{w}_T + \vec{v}_S \tag{3.58}$$

and to check whether $|\vec{w}'_S| < u_{esc_S}(r)$. Then the DM particle will be captured.

In the following, we calculate the probability that a DM particle is captured after scattering by using the previous result.
The downscattering rate can be written as

$$\Omega^-_{u_{esc_S}} = \int_0^{E_{RT}^{max}} dE_{RT} \int_0^{2\pi} d\phi\, |\vec{w}_T|\, n_i(r) \frac{d\sigma}{dE_{RT}\, d\phi}\, \Theta\left(u_{esc_S}(r) - |\vec{w}'_S|\right) \tag{3.59}$$

where

$$\frac{d\sigma}{dE_{RT}\, d\phi} = \frac{1}{2\pi} \frac{1}{E_{RT}^{max}}\, \sigma_{tot}. \tag{3.60}$$

In equation 3.60, we can simply write $\frac{1}{E_{RT}^{max}}$ in front of σ_{tot} since all possible recoil energies, from 0 to E_{RT}^{max}, have the same probability. We can also simply add $\frac{1}{2\pi}$, because the possible values for the free parameter ϕ, between 0 and 2π, have the same probability as well.

The general form of the formula for the capture rate is the same as for the SRF approach, namely

$$C = \sum_i \frac{\rho_H}{m_\chi} \int dV \int d^3u_S \frac{f(\vec{u}_S, \alpha)}{u_S} w_S\, \Omega^-_{u_{esc_S}}(w) \tag{3.61}$$

but the expressions for the downscattering rate $\Omega^{-}_{u_{esc_S}}$, 3.40 and 3.59, are different.

3.3. Summary of the chapter 'Dark matter capture'

In this chapter, we derived the capture formalism where the rotation of stars is considered. To get familiar with this formalism, we first derived the capture formalism as it was used so far, without considering the rotation. After that, we presented two approaches for the modified capture rate, the SRF approach, where we studied the problem fully in the SRF, and the hybrid approach, where we made use of the advantages of both frames, the SRF and TRF. We present the results for both approaches in the following chapter.

4. Results

It was clear from the beginning that the calculations are numerically challenging. To keep the calculation simple in the beginning, we first used two toy models before going to the realistic case. So we got a feeling for the modified capture formalism. We present all these results below in this chapter, but before showing the results, we added a section in which we summarize all the assumptions.

4.1. Assumptions

For the calculations we made several assumptions concerning the properties of the star, DM properties, particle physics, and nuclear physics which we explain in the following.

Properties of the star

We performed this calculation for two kinds of stars, the sun and an O-B-star.

For the **sun**, we have chosen $R = 696 \times 10^6$ m for the radius, and $M = 2 \times 10^{30}$ kg for the total mass [52]. The sun is located at a distance of about 8 kpc to the galactic center and moves with $v_s = 220 \, \frac{km}{s}$ around it [53].

For the **O-B-star**, we assumed $R = 6.6 \times R_\odot$ for the radius and $M = 16 \times M_\odot$ for the total mass. This is the stellar mass and radius that lies in the transition range between O-stars and B-stars. For more detailed information see appendix A. For the distance to the galactic center, we have chosen 0.1 kpc. This short distance is motivated by the "paradox of youth" of stars close to the center of our galaxy, which might be explained by DSs. We have chosen the velocity of the O-B-star around the galactic center to be $v_s = 150 \, \frac{km}{s}$ [53].

For **both stars**, we have chosen the inclination angle α to be $\frac{\pi}{2}$, which means that the rotation axis is perpendicular to the star motion $\vec{v}_s$. We assumed that the total mass of the stars is made of hydrogen, which has atomic mass $m_N = 0.938$ GeV, and that they are rigid bodies, which means that the angular velocity ω is constant throughout the star.

For the nuclei inside the star, we first assumed a number density that is the same in the whole star. The result with this assumption is presented in subsection 4.2.1.

In reality, the number density decreases for larger distances to the center of the star. So our next step was to approximate the number density in the star in a more realistic way. We used the realistic number density from the sun, the solar model AGSS09 [54]. Assuming that the stellar mass is only composed of hydrogen, we had to adapt this model. To keep the calculation still simple, we splitted the star in eleven shells. For each part we used the average number density for this particular shell, as the gray curve in figure 4.1 represents it.

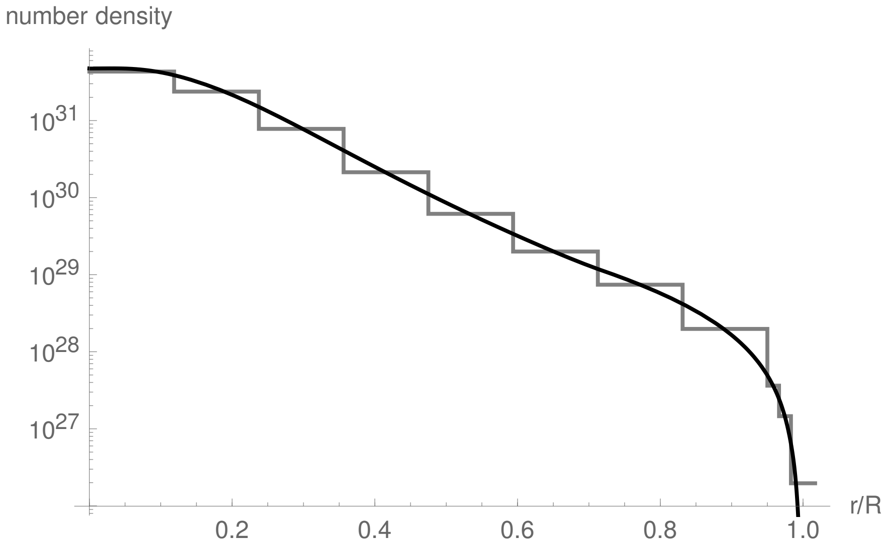

Figure 4.1.: Number density in the star at certain distance to the core normalized with the radius of the star, $\frac{r}{R}$. The black line describes the realistic number density from the solar model AGSS09 adapted for an only-hydrogen star. The gray line is the approximated number density.

The results for this assumption are presented in subsection 4.2.2.

The last step was to use the realistic number density. It is shown as black curve in figure 4.1. The results for this number density are presented in section 4.3.

DM properties

For the DM particles in the galactic halo, we assumed a MBD. The velocity dispersion of DM particles at a distance of 8 kpc is $v_0 = 200 \frac{km}{s}$ and for 0.1 kpc it is $v_0 = 150 \frac{km}{s}$ [55]. Other velocity distributions which we possibly could have taken are briefly explained in appendix D. It was not necessary to take a certain value for the particular local DM halo density. Since we normalize our result for the DM capture rate with the one for the non-rotating case, it cancels out.

Particle physics

We have evaluated the calculation for the three DM masses, namely 100 GeV, 1 TeV and 10 TeV. We have chosen such high masses so that the neutrinos coming from DM annihilations would exceed the threshold of IceCube, $\mathcal{O}\,(100\text{ GeV})$, and DeepCore, $\mathcal{O}\,(10\text{ GeV})$. We assumed velocity independent scattering. Distinguishing between SD and SI scattering was not necessary, since we have normalized all the results with the one for the non-rotating case. As we have additionally assumed that the star is composed of only one element, the scattering cross section cancels out.

Nuclear physics

Since we have only investigated WIMP-proton scattering, we assumed that the form factor $\mid F(q^2) \mid^2 = \exp\left(-\frac{q^2 R_i^2}{3\hbar^2}\right) = 1$.

4.2. Toy models

In this section, we show the results for two different toy models. The following subsections presents our results for the DM capture rate depending on the angular velocity ω for two different assumptions for the number density.

4.2.1. Constant number density inside the star

In this subsection, we are using the same number density throughout the star. Furthermore, we consider the case of the sun and the O-B-star.

Sun

In figure 4.2, we present plots for the sun for $m_\chi = 100$ GeV (top), 1 TeV (middle), and 10 TeV (bottom).

The right plots in figure 4.2 are parts of the left plots where the interesting ω-range for the sun is better resolved to better see a possible increase or decrease of the capture rate in the case of the sun. The red line shows the results obtained from the SRF approach, the dashed purple line was obtained from the hybrid approach. The black dot corresponds to the actual angular velocity of the sun, which is $\omega = 10^{-6}\,\frac{1}{s}$. As we can see very well in the plots for the three assumed DM masses, the capture rate is not significantly changed when we consider an angular velocity as the one for the sun. This is not surprising since the rotational velocity at the equator of the sun is $\approx 2\,\frac{km}{s}$ and the DM particles have at least escape velocity of the sun which is $\mathcal{O}\,(100\,\frac{km}{s})$. So the relative velocity between the nuclei in the sun and the DM particles is only weakly changed by considering the rotation. For $\omega > \mathcal{O}\,(10^{-3}\,\frac{1}{s})$, the capture rate increases rapidly for increasing ω's, but this value is three orders of magnitude larger than the angular velocity of the sun and even larger than the sun's break-up angular velocity.

In the bottom-left plot of figure 4.2, we can see that the SRF and hybrid approach do not agree, possibly due to numerical instabilities. This plot was produced for a high DM mass, namely 10 TeV. The DM mass influences the upper integration limit for the integral over the recoil energy. The maximal possible recoil energy grows and the region over which we must integrate becomes larger. In this case, the SRF approach is more trustable than the hybrid approach.

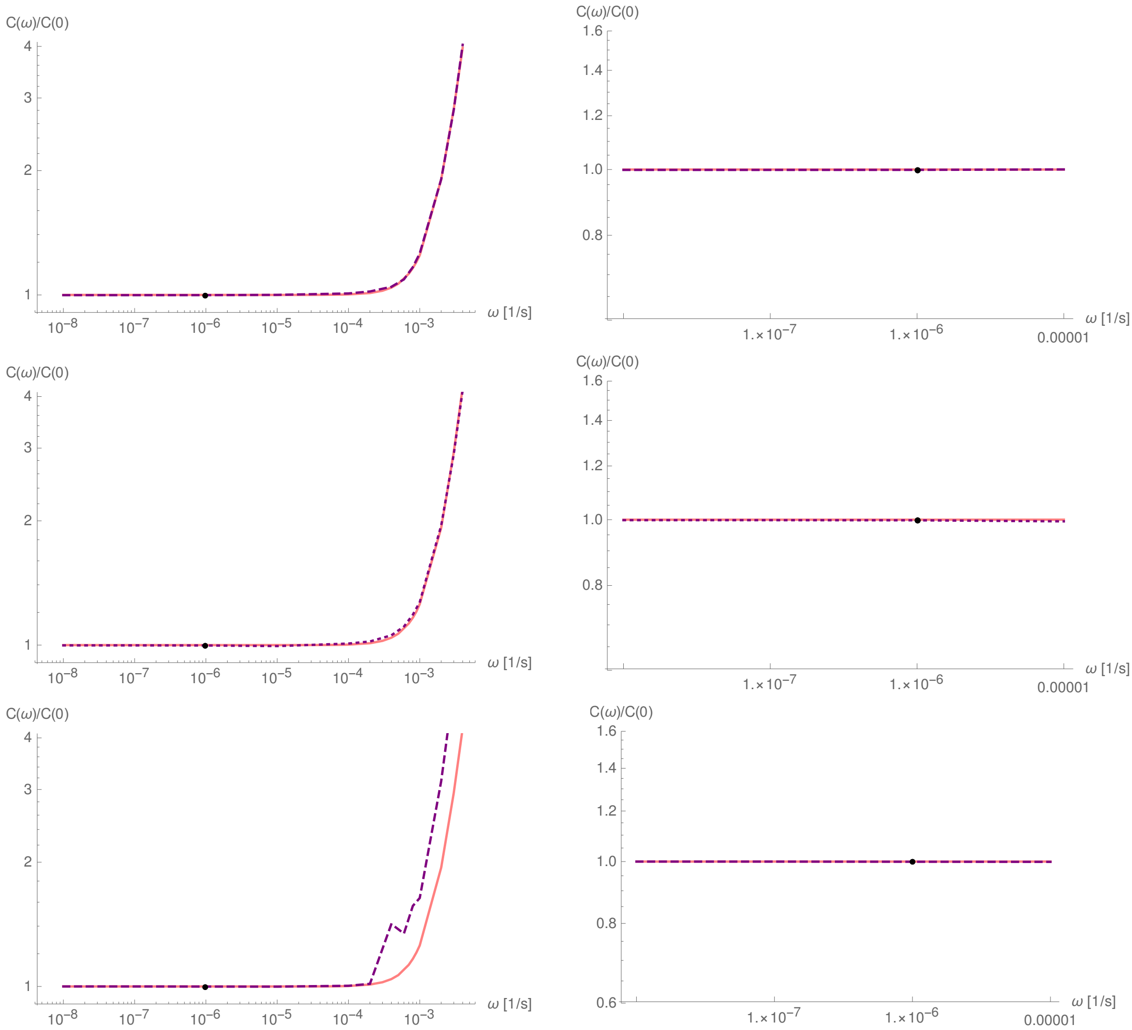

Figure 4.2.: Capture rate for the sun normalized with the capture rate for the non-rotating case, $\frac{C(\omega)}{C(0)}$, vs. angular velocity ω for $m_\chi = 100$ GeV (top), 1 TeV (middle), and 10 TeV (bottom). The number density was assumed to be the same throughout the whole star. The red curve was obtained by using the SRF approach. The dashed purple curve was obtained by using the hybrid approach. The black dot corresponds to the actual angular velocity of the sun, which is $\omega = 10^{-6}\,\frac{1}{s}$. The left plot describes a large ω-range, the right plot describes a short ω-range.

O-B-star

For O-B-stars, the form of the curve looks similar compared to the curves for the sun, see figure 4.3. There, we present the results for $m_\chi = 100$ GeV (top), 1 TeV (middle), and 10 TeV (bottom). The red line represents the SRF approach, whereas the dashed purple line represents the hybrid approach. The black dot corresponds to the angular break-up velocity of the O-B-star, which is $\omega = 2 \cdot 10^{-4}\,\frac{1}{s}$.

The DM capture rate is not significantly influenced by a change in the angular velocity until a value of $\omega = 10^{-4}\,\frac{1}{s}$ is reached. For higher angular velocities, the value for the capture rate increases rapidly. Especially in the left plots of figure 4.3 we can see that rotation indeed can have an influence on the capture rate. The value is enhanced by approximately 15% for $m_\chi = 100$ GeV and 20 % for $m_\chi = 1$ TeV and 10 TeV for the break-up velocity.

Both approaches give basically the same result for $m_\chi = 100$ GeV and 1 TeV. However, as for the case of the sun, the hybrid approach shows numerical instabilities for $m_\chi = 10$ TeV. For this reason, we only show the result for the SRF approach in this case.

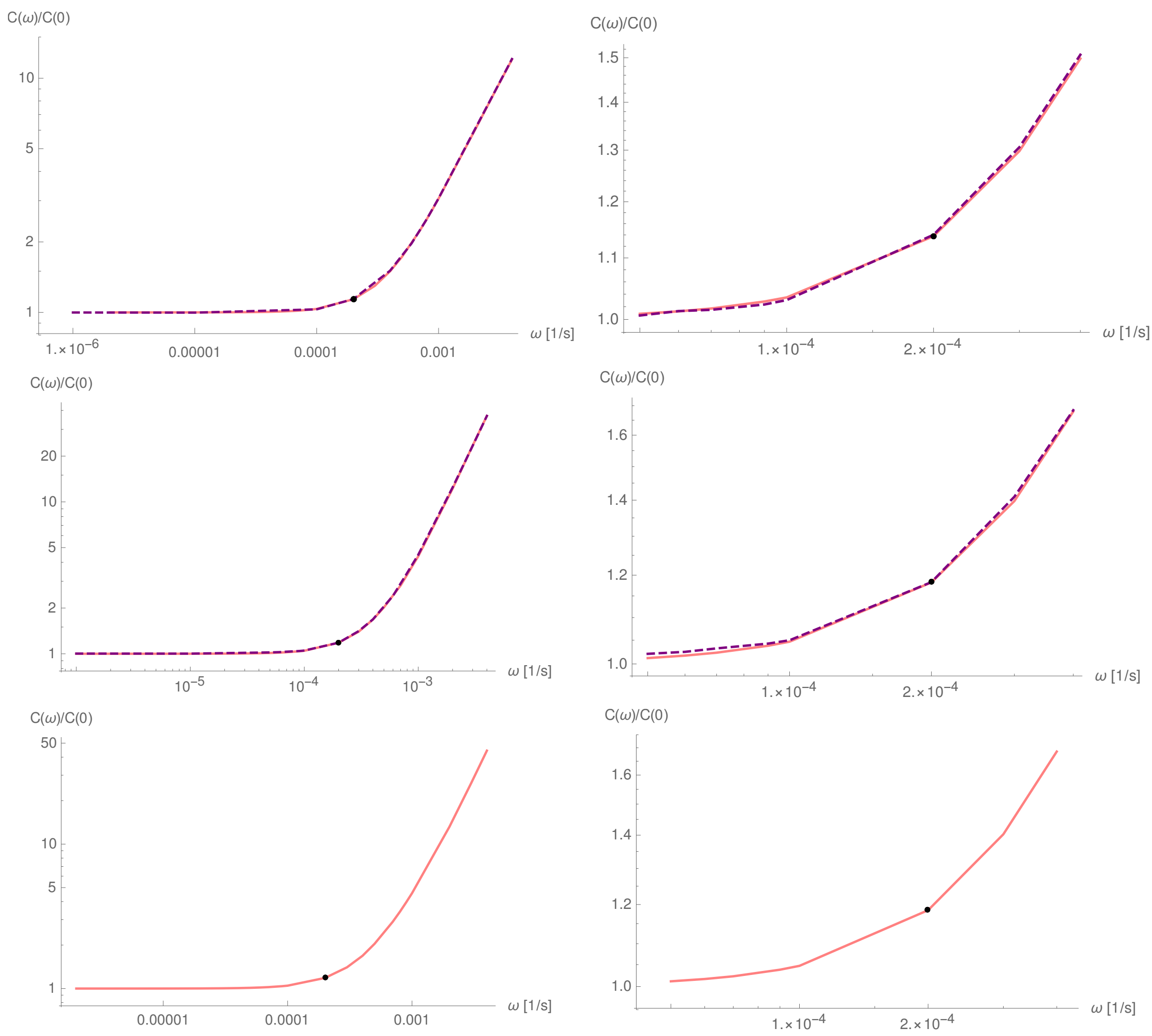

Figure 4.3.: Capture rate for an O-B-star normalized for the capture rate in the non-rotating case, $\frac{C(\omega)}{C(0)}$, vs. angular velocity ω for $m_\chi = 100$ GeV (top), 1 TeV (middle), and 10 TeV (bottom). The number density was assumed to be constant for the whole star. The red curve was obtained by using the SRF approach. The dashed purple curve was obtained by using the hybrid approach. The black dot corresponds to the angular break-up velocity of the O-B-star, which is $\omega = 2 \cdot 10^{-4}\,\frac{1}{s}$. The left plot describes a large ω-range, the right plot describes a short ω-range.

In figure 4.4 we can see that the influence is stronger for heavier DM particles.

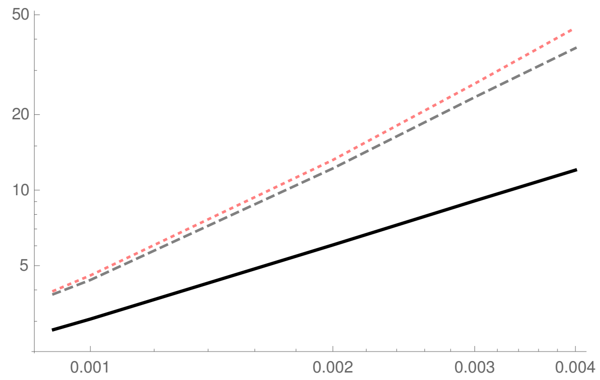

Figure 4.4.: Comparison of the normalized capture rates for an O-B-star using the SRF approach, for $m_\chi = 100$ GeV (black solid line), 1 TeV (gray dashed line) and 10 TeV (red dotted line), and for a constant number density.

A possible explanation for this could be the following. The larger the mass of a DM particle, the larger the energy required to lose in order to be captured, since the minimal energy transfer required for capture writes as $Q_{min} = \frac{1}{2} m_\chi u^2$. So for the DM particles with a large mass only the ones with a very low velocity u can be captured. Otherwise, Q_{min} exceeds the kinematically determined maximal energy transfer Q_{max}. If now the target particles move initially, Q_{max} becomes larger compared to the case where the target particles are at rest, whereas Q_{min} remains unchanged. This effect is enhanced for larger DM masses.

4.2.2. Splitted star with particular average number density

To get a more realistic result, we approximate the density distribution by an "onion-shell" structure with constant density in each shell, as shown in figure 4.1. The gray curve refers to this approximation. As one can see, we still assume a constant number density, but not the same for the whole star. We again present results for the sun and an O-B-star. We limit ourselves on the case for $m_\chi = 1$ TeV and the SRF approach owing to the long computation times.

Sun

Figure 4.5 shows the results of the capture rate for the sun for $m_\chi = 1\,TeV$.

We obtained a curve with a form similar to one in subsection 4.2.1, but the increase is less rapid here. Even for large ω's the effect of the rotation is very small compared to the curves for the constant number density. This lower effect of rotation for a more realistic number density is not very surprising. Assuming the same number density throughout the whole star, we strongly overestimate the outer regions of the star where the effect of the rotation should be the largest.

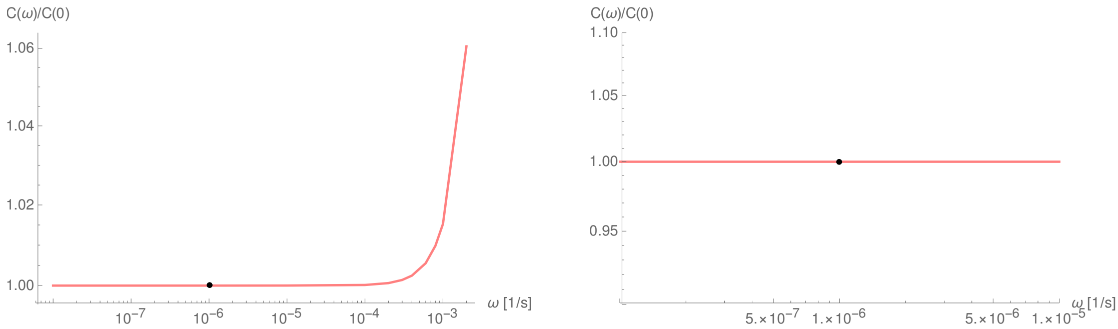

Figure 4.5.: Capture rate for the sun normalized with the capture rate for the non-rotating case, $\frac{C(\omega)}{C(0)}$, vs. angular velocity ω for $m_\chi = 1$ TeV. The number density was approached as one can see in figure 4.1 (gray curve). We used the SRF approach. The black dot corresponds to the actual angular velocity of the sun, which is $\omega = 10^{-6}\,\frac{1}{s}$. The left plot describes a large ω-range, the right plot describes a short ω-range.

O-B-star

The same holds for the O-B-star, as we can see in figure 4.6.

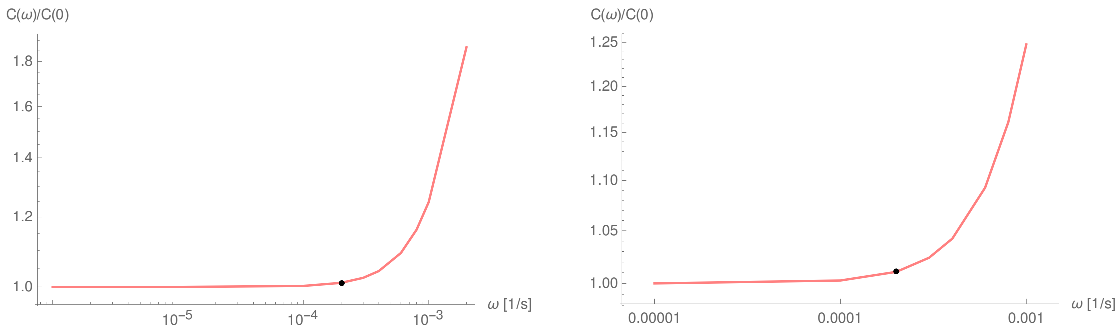

Figure 4.6.: Capture rate for the O-B-star normalized with the capture rate for the non-rotating case, $\frac{C(\omega)}{C(0)}$, vs. angular velocity ω for $m_\chi = 1$ TeV. The number density was approached as one can see in figure 4.1 (gray curve). We used the SRF approach. The black dot corresponds to the angular break-up velocity of the O-B-star, which is $\omega = 2 \cdot 10^{-4}\,\frac{1}{s}$. The left plot describes a large ω-range, the right plot describes a short ω-range.

As in the case of the sun, the impact of the rotation on the DM capture rate is reduced compared to the case with the constant number density.

4.3. Realistic number density

Our final and most important result is presented in this section. Here, we finally use the realistic number density for the sun and the O-B-star. However, it is important to mention again that we have assumed that the star is composed only of hydrogen, with a density distribution as given by the solar model AGSS09, which is shown as black curve in figure 4.1. We again limit ourselves on the case for $m_\chi = 1$ TeV and the SRF approach.

Sun

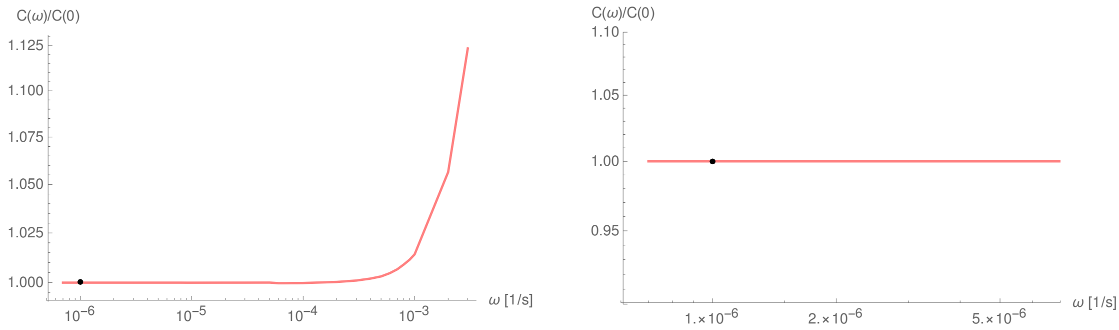

Figure 4.7.: Capture rate for the sun normalized with the capture rate for the non-rotating case, $\frac{C(\omega)}{C(0)}$, vs. angular velocity ω for $m_\chi = 1$ TeV. We assumed a realistic number density as one can see in figure 4.1 (black curve). The red curve was obtained by using the SRF approach. The black dot corresponds to the actual angular velocity of the sun, which is $\omega = 10^{-6}\,\frac{1}{s}$. The left plot describes a large ω-range, the right plot describes a short ω-range.

The result in figure 4.7 is similar to the result in subsection 4.2.2. Considering the realistic number density, there is no visible effect of the rotation on the capture rate of the sun. We again have only a significant increase in the capture rate for ω's larger than $\approx 10^{-3}\,\frac{1}{s}$, which exceed the angular break-up velocity for sunlike stars.

O-B-star

For the O-B-star the result is also similar to the one in subsection 4.2.2, as we can see in figure 4.8.

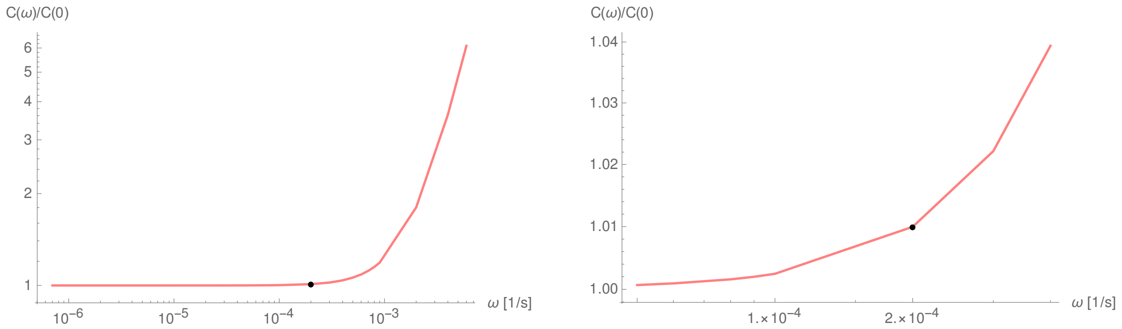

Figure 4.8.: Capture rate for an O-B-star normalized with the capture rate for the non-rotating case, $\frac{C(\omega)}{C(0)}$, vs. angular velocity ω for $m_\chi = 1$ TeV. We assumed a realistic number density as one can see in figure 4.1 (black curve). The red curve was obtained by using the SRF approach. The black dot corresponds to the angular break-up velocity of the O-B-star, which is $\omega = 2 \cdot 10^{-4}\,\frac{1}{s}$. The left plot describes a large ω-range, the right plot describes a short ω-range.

For an O-B-star, a small increase of the capture rate due to rotation is possible if ω is close to the break-up angular velocity. Higher angular velocities are again physically impossible.

5. Conclusions

DM particles in the galactic halo which are travelling through a star can scatter off a nuclei in the star and transfer energy to them. If the energy transfer is sufficiently high, the DM particles get captured and can accumulate at the core of the star via multiple scattering. Reaching a sufficiently high DM density inside the star, the DM particles can annihilate efficiently. The annihilation products which are trapped inside the star provide another energy source, besides nuclear fusion, for the star system and might influence the stellar evolution. The produced neutrinos however, which leave the star almost unhindered, could be detected by neutrino telescopes like IceCube. In the DM capture formalism that was used so far, one neglects the rotation of stars. The goal of this project was to analyze the impact of stellar rotation on the DM capture rate by paying particular attention to the sun, which is the star closest to us, and O-B-stars close to the galactic center. Investigating the influence on O-B-stars was motivated by the fact that this class of stars can have large rotational velocities, and by the "paradox of youth" which might be explained by an efficient energy injection into the star caused by the annihilation of captured DM particles.

We have presented two approaches to determine the DM capture rate considering the stellar rotation. For the first approach, the SRF approach, we fully stayed in the SRF, whereas we used the advantages of both frames, the simple form of the escape velocity in the SRF and the well known cross section in the TRF, for the second approach, the hybrid approach.

We have investigated the DM capture rate for $m_\chi = 100$ GeV, 1 TeV, and 10 TeV for the constant number density, and $m_\chi = 1$ TeV for the realistic number density, as given by the solar model AGSS09, by using the presented approaches, where stellar rotation is considered. For both, the sun and the O-B-star, we have assumed that they are only composed of hydrogen.

Assuming that the number density of nuclei is the same throughout the star, we found that the DM capture is not significantly changed for the sun when we take stellar rotation into account. For the O-B-star rotating with break-up velocity, we obtained an increase in the DM capture rate of $\approx$ 15 % for $m_\chi = 100$ GeV, and $\approx$ 20 % for $m_\chi = 1$ TeV and 10 TeV.

Assuming a realistic number density of nuclei, we again obtained no significant change in the DM capture rate in the case of the sun. For the O-B-star, the DM capture rate still increases for larger angular velocities, but less rapidly as in the case of the constant number density. If this star rotates with break-up velocity, the increase is $\approx$ 1 %.

The DM capture rate is not significantly affected by rotation, so we conclude that there are no changes for IceCube concerning the neutrino flux produced by DM annihilations inside the sun.

The effect on the O-B-star rotating with break-up velocity is $\approx$ 1 %. This means that rather no effect on the stellar evolution by a change in the DM capture rate can be seen.

6. Outlook

There are several improvements for the evaluation of the modified capture formalism concerning the properties of the star, particle physics, and nuclear physics which we defer to the future.

An improvement for the *properties of the star* will be to take all appearing elements inside the star into account, since the assumption that a star only consists of hydrogen describes the star poorly. Also the number density distribution of the O-B-star has to be improved. The solar model AGSS09 is a good description for the nucleon density distribution inside the sun, but the O-B-stars have a completely different nucleon density profile than the sun, so the one assumed in this work has to be adapted.

Also the *particle physics* aspects can be improved. If we now take all elements inside the star into account, we have to perform the calculation for SD and SI scattering. The impact for SI scattering could be especially large, as the dominant contribution to the capture rate in this case comes from oxygen and helium-4, and not from hydrogen [56]. Further, it was shown in various concrete particle models for DM that the scattering cross section could be dependent on the momentum transfer or on the velocity [57]. So one could evaluate the calculations also for these kinds of cross sections. In this work, we have considered DM masses higher than 100 GeV, because of the IceCube threshold. But it would also be interesting to check, how the stellar rotation influences the DM capture rate for lower DM masses, since we cannot exclude the possibility of a decrease in the DM capture rate for high angular velocities assuming a lower DM mass. The best limits of indirect detection experiments for $m_\chi < 20$ GeV provides SuperK [16, 17].

By taking into account also heavier elements than hydrogen, the nuclear form factor cannot be set equal to 1 anymore. So also the assumptions for *nuclear physics* can be improved.

As we can see with the help of the both used examples, sun and O-B-star, it is clear that the DM capture rate of some kinds of stars are stronger influenced by stellar rotation than others. For this reason, it would be sensible to take also other kinds of stars into account and to evaluate the modified capture formalism for them.

Other objects of interest for the detection of DM via capture could be neutron stars (NS). To calculate capture rates for NSs by considering rotation, this capture formalism has to be adapted since NSs are compact objects with a high mass which makes them relativistic. This fact causes strong forces, high accelerations and therefore relativistic velocities of the incoming DM particles. In order to have a small relative velocity between the incoming DM particles and the neutrons, the value for the angular momentum has to be comparatively high. Besides, in the non-relativistic case, the escape velocity can be derived by using Newtonian gravity, but for NSs we have to take General Relativity into account. In addition, the other composition of NSs has to be considered. This consists, as the name implies, essentially of neutrons, but for example also of ions and electrons in the outer layers [58]. Also the cross section has to be treated carefully since the DM velocity at the time of scattering is relativistic.

One idea of how NSs can be influenced by captured DM, and therefore also by considering the rotation, is the NS heating by DM which annihilates inside the NS [59]. In this scenario, the products of DM annihilation transfer their energy to the neutrons in the NS. This energy is not enough to counteract the NS's gravity, but it may generate a glow which prohibits the NS to cool out completely. If the rotation affects the DM capture rate significantly, the glow caused by DM annihilation changes.

Another probe for DM are pulsars. Pulsars are highly magnetized NSs which emit a electromagnetic beam of radiation. In [60, 61], the authors propose that a sufficient dense core of DM particles in a pulsar could create a black hole (BH) which causes the implosion of the NS. This leads to a maximal lifetime for the NS. If its rotation enhances the capture, the lifetime of the NS will though be shortened.

Appendices

A. Advantages of O-B-stars

Choosing a suitable star is important to see what effect rotation has on the DM capture rate. In the following three kinds of stars are presented.

Since the sun is the star closest to us, it would be natural to check the influence of stellar rotation on the DM capture rate for this star. The rotational velocity of the sun at the equator is about $2\,\frac{km}{s}$ [62]. The DM particles in the Milky Way reach velocities of several hundred kilometers per second [55]. The relative velocity of the target particles (the nuclei in the sun) and the DM particles would not greatly differ from the velocity of the DM particles, which means that in the case of the sun, the rotation probably has a vanishingly small influence on the capture rate. Therefore, one should also consider celestial bodies that have a higher rotational velocity than the sun. However, we also applied the modified capture formalism to the sun in order to see if considering the rotation has at least a small effect.

Very fast rotating objects in the universe are, for example, NSs. One of the NS closest to us is PSR J0108-1431 [63]. Its rotation period is 0.808 s, whereby its rotation velocity at the equator is an order of magnitude larger than that of the sun. But NSs can rotate even faster. The fastest spinning NS known is PSR J1748-2446ad [64]. This rotates 716 times a second, which is equivalent to a rotation velocity of about 0.24 c at the equator. For NSs it is necessary that they rotate rapidly in order to see a signficiant effect of stellar rotation. Due to their compactness and high mass, the NS accelerates the DM particles to relativistic velocities before the DM particles have the chance to interact with the target particles. If the DM particles move at a relativistic velocity and the NS rotates comparatively slowly, the relative velocity between the target particles and the DM particles hardly differs from the velocity of the DM particles, as in the case of the sun. Thus, the rotation again might not influence the capture rate. Additionally, the modified capture formalism in this work has to be adapted for relativistic velocities. Promising candidates are the so-called O-B-stars.

Stars can be divided into different groups using their spectral characteristics. They are classified by using the letters *O, B, A, F, G, K* and *M* (optionally with numeric subdivision), from O being hottest and M being coolest [65]. These stars can not only be assigned a special temperature range but also a mass and radius range. O-stars have masses of more than 16 $M_\odot$ and a radius of more than 6.6 $R_\odot$ [66], whereas B-stars are smaller and have less mass. These have a mass in the range of 2.1 - 16 $M_\odot$ and a radius of 1.8 - 6.6 $R_\odot$ [67].

Regulus [32, 68], which is located approximately 79 ly from the sun, is a multiple star system which consists of four stars, where Regulus A is the dominant star. Regulus A is a binary system with a satellite star of 0.3 $M_\odot$ and a blue-white main-sequence star of type B [69]. Regulus is interesting because, with a mass of 3.8 $M_\odot$ [70], a radius of 3.1 $R_\odot$ [68] and a projected rotational velocity (see appendix E for a definition) of 320 $\frac{km}{s}$ [71], which is three orders of magnitudes larger than the rotational velocity of the sun, it provides optimal conditions to study the influence of the rotation on the capture rate. The rotation velocity fits well with the velocity of the DM particles, which are not accelerated to relativistic velocities since this star is not massive and compact enough, as NSs are. This rotation velocity is extremely high for a star of this type and it is worth noting that it has 96.5 % of the critical angular velocity for break-up.

B. Definition of variables and indices

Here, we explain different variables and abbrevations that we use in this thesis.

$\vec{u}$: velocity of the incoming DM particle infinitely far away from the star
$u_{esc}(r)$: escape velocity at the distance r to the center of the star
$\vec{w}(r)$: velocity of the DM particle at the collision point r before scattering, accelerated by the gravitational field of the star, $w^2(r) = u^2 + u_{esc}^2(r)$
$\vec{w}'(r)$: velocity of the DM particle at the collision point r after scattering

ω: angular velocity of the nuclei inside the star
$v = \rho\omega$: velocity of the target particles inside the star at distance ρ to rotation axis of the star before scattering
v': velocity of the target particles inside the star after scattering

v_s: velocity of the star around the galactic center
v_0: velocity dispersion of the MBD

The indices denote the following:
G: galactic rest frame (GRF)
S: star rest frame (SRF)
T: target rest frame (TRF)

Further abbreviations we use frequently:
DM: dark matter
χ: designation index for dark matter in connection with a variable
DS: Dark Star
SM: standard model
NS: neutron star

C. DM annihilation rate and DM abundance in the star

After DM particles have been captured and have accumulated in the core in a sufficiently high amount to have a high DM density, the DM particles can start to self-annihilate efficiently. The annihilation rate can be written as [72]

$$\Gamma_A = \frac{1}{2} C_A N^2 \tag{C.1}$$

where C_A is the annihilation constant and N is the number of DM particles. Besides capture and annihilation, there is another process that influences the number of DM particles inside the star, namely evaporation [73, 74]. Captured DM particles can gain energy when they rescatter with nuclei in the star. If they gain enough energy to have a larger velocity than the local escape velocity in the end, they can escape from the star. The change of the number of DM particles inside a star is then determined by capture, evaporation and annihilation and can be written as [72]

$$\frac{dN}{dt} = C - C_E N - C_A N^2 \tag{C.2}$$

where C_E is the evaporation rate. In [75], they elaborated that for the sun DM evaporation is important for DM masses of $m_\chi = 1 - 4$ GeV. We investigate DM masses of $\mathcal{O}\,(100 \text{ GeV})$ or higher. So we neglect evaporation in the following. Assuming that there were no WIMPs inside the star in the beginning, $n\,(t = 0) = 0$, and neglecting evaporation, equation C.2 can be solved with

$$N(t) = \sqrt{\frac{C}{C_A}} \tanh\left(\frac{t}{\tau}\right) \tag{C.3}$$

where $\tau = \frac{1}{\sqrt{C\,C_A}}$ is the equilibration time. If $t >> \tau$, the number of DM particles does not change anymore. This means that an equilibrium between capture and annihilation sets in. So when equilibrium is reached

$$\tanh\left(\frac{t}{\tau}\right) \approx 1, \tag{C.4}$$

and equation C.3 simplifies to

$$N(t) = \sqrt{\frac{C}{C_A}}. \tag{C.5}$$

By plugging in C.1 in C.5, we obtain

$$\Gamma_A = \frac{C}{2}. \tag{C.6}$$

This equation is valid when equilibrium is reached, and tells us that after the capture of two DM particles, one DM annihilation (of two DM particles) follows.

D. DM velocity distributions

To determine the DM velocity distribution in galaxies, one needs to know the DM density profile. There are several different density profiles. First, one assumed that the DM distribution was that of the Standard Halo [76]. In this model, the DM particles are distributed in the galaxy after the singular isothermal sphere (SIS) profile

$$\rho_{SIS}(r) = \frac{v_0^2}{2\pi\, G\, r^2} \tag{D.1}$$

where v_0 is the velocity dispersion. In the past years, it became clear that the SIS profile describes the DM halo not good enough. E.g. [77, 78, 79] show numerical simulations that confirm this.
In the following, three different DM density profiles are presented.

D.1. DM density profiles

In the following subsection, we present the Navarro-Frenk-White (NFW), Einasto and Burkert profile.

Navarro-Frenck-White profile
The (cusped) NFW density profile [79] can be expressed by

$$\rho_{NFW} = \frac{\rho_0}{\frac{r}{r_s}\left(1 + \frac{r}{r_s}\right)^2} \tag{D.2}$$

where $r_s = 20$ kpc is the scale radius.

Einasto profile
An alternative density profile that provides a less steep rise of the DM density near the galactic center is the Einasto profile [80] which can be written as

$$\rho_{Ein} = \rho_0 \exp\left(-\frac{2}{\gamma}\left[\left(\frac{r}{r_s}\right)^{\gamma} - 1\right]\right) \tag{D.3}$$

where $r_s = 20$ kpc is again the scale radius. The value γ is chosen to be 0.17 since it fits galactic- and cluster-sized halos in N-body simulations very well [81, 82].

Burkert profile
In contrast to the NFW profile, which provides a poor fit for dwarf galaxies, the Burkert profile is a cored density profile that describes dwarf galaxies quite well [83]. It is given by the density

$$\rho_{Bur} = \frac{\rho_0}{\left(1 + \frac{r}{r_s}\right)\left(1 + \frac{r^2}{r_s^2}\right)}. \tag{D.4}$$

In this case, the scale radius $r_s = 650$ pc was chosen, which fits the kinematics of Draco [84].

The velocity distribution is associated with the density profile.

D.2. DM velocity distributions in comparison

One way to get the velocity distribution from the density profile was shown in the paper [55].

In the following, we briefly review the calculation. One necessary formula to obtain the velocity distribution is Eddington's equation

$$F(\tilde{\epsilon}) = \frac{1}{8\sqrt{2}\,\pi^3\sqrt{G^3\, r_{vir}^3\, M_{vir}}}\frac{1}{g(c)} \times \tilde{F}(\tilde{\epsilon}), \tag{D.5}$$

where

$$\tilde{F}(\tilde{\epsilon}) = \int_0^{\tilde{\epsilon}} \frac{d\tilde{\psi}}{\sqrt{\tilde{\epsilon} - \tilde{\psi}}}\frac{d^2\tilde{\psi}}{d\tilde{\psi}^2}. \tag{D.6}$$

A tilde indicates a dimensionless quantity.

The virial radius r_{vir} is defined such that the average density contained in a sphere with volume $\frac{4}{3\,\pi\, r_{vir}^3}$ is $\approx$ 200 times the critical mass of the universe. M_{vir} is then the mass contained in this sphere. The concentration parameter is defined as $c = \frac{r_{vir}}{r_s}$. Here, $\tilde{\psi}$ is the dimensionless relative potential

$$\tilde{\psi} = \frac{r_{vir}}{G\, M_{vir}}\,\psi, \quad \psi = -\Phi \tag{D.7}$$

where Φ is the gravitational potential per unit mass, and $\tilde{\epsilon}$ is the dimensionless relative energy

$$\tilde{\epsilon} = \frac{r_{vir}}{G\, M_{vir}}\,\epsilon, \quad \epsilon = \psi - \frac{v^2}{2}. \tag{D.8}$$

Using D.5 and D.6, we can write the three-dimensional velocity distribution function as

$$f_{\vec{x}}(\vec{v})\, d\vec{v} = \frac{1}{\sqrt{8}\pi^2}\sqrt{\left(\frac{r_{vir}}{G\, M_{vir}}\right)^3}\frac{\tilde{F}\left(\psi - \frac{v^2}{2}\right)}{\tilde{\rho}(\vec{x})}. \tag{D.9}$$

The one-dimensional velocity distribution of the magnitude of the velocity takes the form

$$f_r(v^2)\,dv \;=\; \frac{\sqrt{2}}{\pi}\sqrt{\left(\frac{r_{vir}}{G\,M_{vir}}\right)^3}\,v^2\,\frac{\tilde{f}}{\tilde{\rho}}\,dv. \tag{D.10}$$

Figures D.1, D.2 and D.3 compare the velocity distributions obtained by the NFW, Einasto and Burkert profiles with MBD. I created these plots for my Bachelor's thesis, following [55].

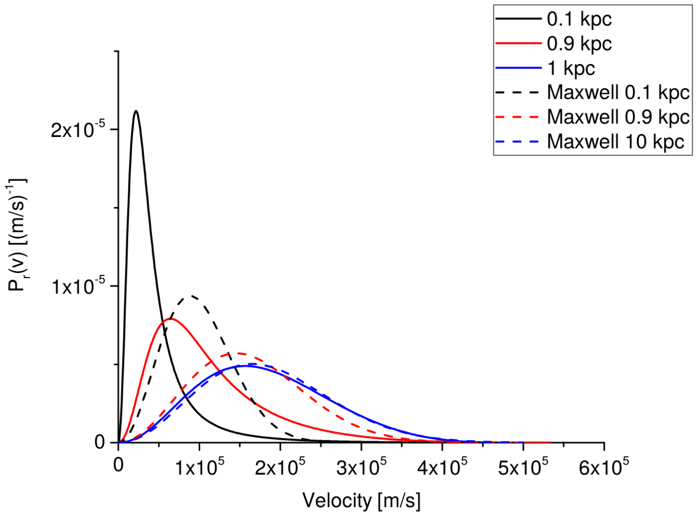

Figure D.1.: Comparison of the velocity distribution obtained by the NFW profile and the MBD for different distances to the galactic center. Equation D.10 was used and baryons weren't considered. The same-colored, dotted lines refer to the corresponding MBD with the same velocity dispersion as for the NFW velocity distribution.

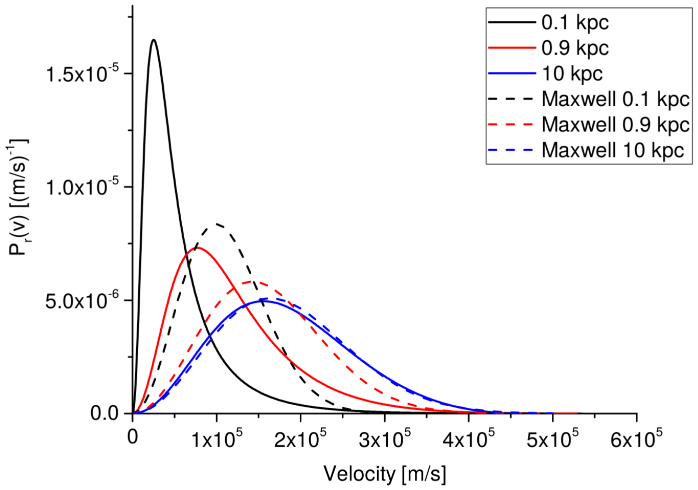

Figure D.2.: Comparison of the velocity distribution obtained by the Einasto profile and the MBD for different distances to the galactic center. Equation D.10 was used and baryons weren't considered. The same-colored, dotted lines refer to the corresponding MBD with the same velocity dispersion as for the Einasto velocity distribution.

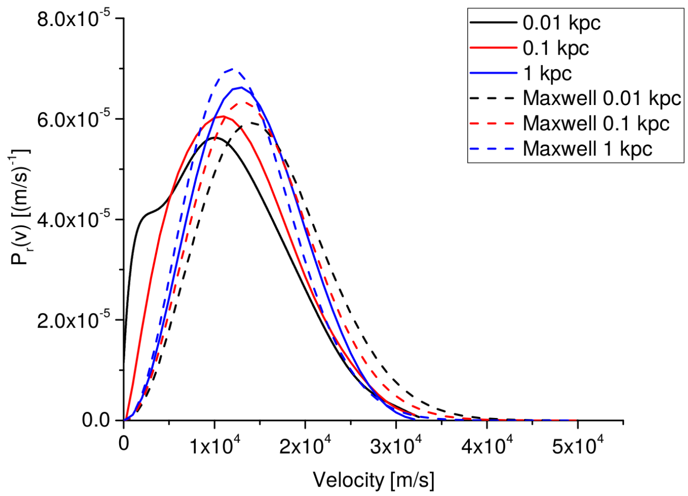

Figure D.3.: Comparison of the velocity distribution obtained by the Burkert profile for a classical dwarf galaxy and the MBD for different distances to the galactic center. Equation D.10 was used and baryons weren't considered. The same-colored, dotted lines refer to the corresponding MBD with the same velocity dispersion as for the Burkert velocity distribution.

In the figures D.1, D.2 and D.3, we can see the velocity distribution for three different distances to the galactic center. To create these figures, the designation $P_r(v)$ was used for the velocity distribution, instead of $f(u)$, which we actually use in this work.

For larger distances to the galactic center, figure D.1 and D.2 show that MBD fits the NFW and Einasto profile very well. For smaller distances, however, the difference becomes larger.

For dwarf galaxies and the Burkert velocity distribution, the MBD is an even worser fit for smaller distances, as one can see in D.3.

E. Measurement of the stellar rotation velocity

Usually, the rotation axis of a star is inclined by an angle i to the line of sight. This means that the real equatorial rotation velocity v_{rot} cannot be measured directly. The observed rotation velocity, also called "projected rotational velocity", of the star is $v_o = v_{rot}\sin(i)$. Figure E.1 clarifies the problem. The velocity v_o can be determined spectroscopically [85].

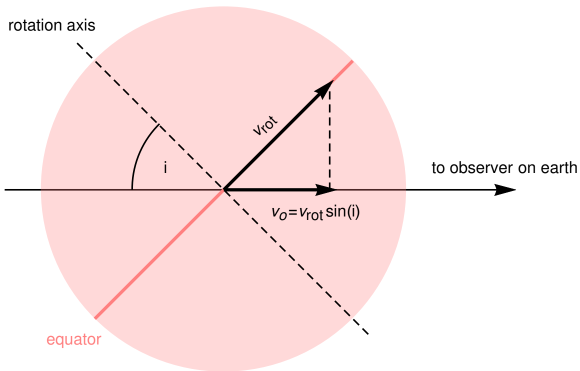

Figure E.1.: Equatorial and projected rotation velocity

For the determination of v_o one uses the Doppler effect. For this, one takes the spectrum from stars. It is known how broad the absorption lines of the certain star is. Since the star is rotating, there are regions where the emitted light is red-shifted and there are regions where the light is blue-shifted (if the inclination angle i is not 0). This means that the faster a star rotates, the broader the absorption line will be. Depending on how broad the absorption line is, one can deduce the projected rotation velocity. But if the inclination i is not known, v_{rot} cannot be determined. However, v_o gives at least a lower limit for the rotation velocity v_{rot}.

F. Escape velocity in the target rest frame

The position of the target in the SRF is given by

$$\vec{x}_{N_S}(t) = \begin{pmatrix} \rho \cos(\omega t) \\ \rho \sin(\omega t) \\ z \end{pmatrix} = \begin{pmatrix} \rho \cos \varphi \\ \rho \sin \varphi \\ z \end{pmatrix}. \tag{F.1}$$

The velocity of the targets in the SRF is then given by

$$\vec{v}_S \equiv \dot{\vec{x}}_{N_S}(t) = \begin{pmatrix} -\rho\,\omega \sin(\omega t) \\ \rho\,\omega \cos(\omega t) \\ 0 \end{pmatrix} = \begin{pmatrix} -\rho\,\omega \sin \varphi \\ \rho\,\omega \cos \varphi \\ 0 \end{pmatrix} \tag{F.2}$$

which is also the velocity of the TRF.

The boosted velocity of the DM particles in the GRF is

$$\vec{w}_G = \begin{pmatrix} w_G \sin\theta_u \cos\varphi_u \\ w_G \sin\theta_u \sin\varphi_u \\ w_G \cos\theta_u \end{pmatrix} \tag{F.3}$$

and the velocity of the star in the GRF is

$$\vec{v}_{s_G} = \begin{pmatrix} v_{s_G} \sin \alpha \\ 0 \\ v_{s_G} \cos \alpha \end{pmatrix} \tag{F.4}$$

where α is defined as the angle between the z-axis and $\vec{v}_{s_G}$.

The velocity of the DM particles in the SRF is

$$\vec{w}_S = \begin{pmatrix} -v_{s_G} \sin \alpha + w_G \sin \theta_u \cos \varphi_u \\ w_G \sin \theta_u \sin \varphi_u \\ -v_{s_G} \cos \alpha + w_G \cos \theta_u \end{pmatrix} \tag{F.5}$$

which is the relative velocity of the star and the DM particle in the GRF.

The velocity of the DM particles in the TRF is

$$\vec{w}_T = \begin{pmatrix} \rho\,\omega\,\sin\varphi + v_{s_G}\,\sin\alpha - w_G\,\sin\theta_u\,\cos\varphi_u \\ -\rho\,\omega\,\cos\varphi - w_G\,\sin\theta_u\,\sin\varphi_u \\ v_{s_G}\,\cos\alpha - w_G\,\cos\theta_u \end{pmatrix} \tag{F.6}$$

which is the relative velocity between the SRF and the DM particles in the SRF.

That a DM particle can just escape,

$$\mid u_{esc_S} \mid = \mid \vec{w}_S \mid = \mid \vec{w}_T + \vec{v}_S \mid = \sqrt{v_T^2 + w_T^2 + 2\,w_T\,v_S\,\cos\left(\vec{w}_T, \vec{v}_S\right)} \tag{F.7}$$

must be fulfilled.
Solving F.7 for w_T provides the two solutions

$$w_{T_1} = -\,v_S\,\cos\left(\vec{w}_T, \vec{v}_S\right) + \sqrt{u_{esc_S}^2 + v_S^2\left(\cos^2\left(\vec{w}_T, \vec{v}_S\right) - 1\right)} \tag{F.8}$$

$$w_{T_2} = -\,v_S\,\cos\left(\vec{w}_T, \vec{v}_S\right) - \sqrt{u_{esc_S}^2 + v_S^2\left(\cos^2\left(\vec{w}_T, \vec{v}_S\right) - 1\right)}. \tag{F.9}$$

The values for the solution F.9 are negative. So I drop this solution and use F.8.
The direction dependent escape velocity in the TRF is then defined by

$$u_{esc_T} = -\,v_S\,\cos\left(\vec{w}_T, \vec{v}_S\right) + \sqrt{u_{esc_S}^2 + v_S^2\left(\cos^2\left(\vec{w}_T, \vec{v}_S\right) - 1\right)}. \tag{F.10}$$

Bibliography

[1] J. H. Oort. “The force exerted by the stellar system in the direction perpendicular to the galactic plane and some related problems”. In: 6 (Aug. 1932), p. 249.

[2] F. Zwicky. “Die Rotverschiebung von extragalaktischen Nebeln”. In: *Helv. Phys. Acta* 6 (1933). [Gen. Rel. Grav.41,207(2009)], pp. 110–127. DOI: 10.1007/s10714-008-0707-4.

[3] F. Zwicky. “On the Masses of Nebulae and of Clusters of Nebulae”. In: *Astrophys. J.* 86 (1937), pp. 217–246. DOI: 10.1086/143864.

[4] Guido Cupani, Marino Mezzetti, and Fabio Mardirossian. “Cluster mass estimation through fair galaxies”. In: *Monthly Notices of the Royal Astronomical Society* 403.2 (2010), pp. 838–847.

[5] Katherine Freese. “Status of Dark Matter in the Universe”. In: *Int. J. Mod. Phys.* 1.06 (2017), pp. 325–355. DOI: 10.1142/S0218271817300129, 10.1142/9789813226609_0018. arXiv: 1701.01840 [astro-ph.CO].

[6] P. A. R. Ade et al. “Planck 2013 results. I. Overview of products and scientific results”. In: *Astron. Astrophys.* 571 (2014), A1. DOI: 10.1051/0004-6361/201321529. arXiv: 1303.5062 [astro-ph.CO].

[7] M. R. Nolta et al. “Five-Year Wilkinson Microwave Anisotropy Probe (WMAP) Observations: Angular Power Spectra”. In: *Astrophys. J. Suppl.* 180 (2009), pp. 296–305. DOI: 10.1088/0067-0049/180/2/296. arXiv: 0803.0593 [astro-ph].

[8] Vera C. Rubin, W. Kent Ford Jr., and Norbert Thonnard. “Extended rotation curves of high-luminosity spiral galaxies. IV. Systematic dynamical properties, Sa through Sc”. In: *Astrophys. J.* 225 (1978), pp. L107–L111. DOI: 10.1086/182804.

[9] Mariangela Lisanti. “Lectures on dark matter physics”. In: *New Frontiers in Fields and Strings: TASI 2015 Proceedings of the 2015 Theoretical Advanced Study Institute in Elementary Particle Physics*. World Scientific, 2017, pp. 399–446.

[10] Gary Steigman, Basudeb Dasgupta, and John F. Beacom. “Precise Relic WIMP Abundance and its Impact on Searches for Dark Matter Annihilation”. In: *Phys. Rev.* D86 (2012), p. 023506. DOI: 10.1103/PhysRevD.86.023506. arXiv: 1204.3622 [hep-ph].

[11] Volker Springel et al. “Simulations of the formation, evolution and clustering of galaxies and quasars”. In: *nature* 435.7042 (2005), p. 629.

[12] Xiangyi Cui et al. “Dark Matter Results From 54-Ton-Day Exposure of PandaX-II Experiment”. In: *Phys. Rev. Lett.* 119.18 (2017), p. 181302. DOI: 10.1103/PhysRevLett.119.181302. arXiv: 1708.06917 [astro-ph.CO].

[13] D. S. Akerib et al. “Calibration, event reconstruction, data analysis, and limit calculation for the LUX dark matter experiment”. In: *Phys. Rev.* D97.10 (2018), p. 102008. DOI: 10.1103/PhysRevD.97.102008. arXiv: 1712.05696 [physics.ins-det].

[14] J. Schieck et al. “Direct Dark Matter Search with the CRESST II Experiment”. In: *PoS* ICHEP2016 (2016), p. 217. DOI: 10.22323/1.282.0217. arXiv: 1611.02113 [astro-ph.CO].

[15] E. Aprile et al. “Dark Matter Search Results from a One Ton-Year Exposure of XENON1T”. In: *Phys. Rev. Lett.* 121.11 (2018), p. 111302. DOI: 10.1103/PhysRevLett.121.111302. arXiv: 1805.12562 [astro-ph.CO].

[16] C. Amole et al. “Dark Matter Search Results from the PICO-60 C_3F_8 Bubble Chamber”. In: *Phys. Rev. Lett.* 118.25 (2017), p. 251301. DOI: 10.1103/PhysRevLett.118.251301. arXiv: 1702.07666 [astro-ph.CO].

[17] M. G. Aartsen et al. “Search for annihilating dark matter in the Sun with 3 years of IceCube data”. In: *Eur. Phys. J.* C77.3 (2017), p. 146. DOI: 10.1140/epjc/s10052-017-4689-9. arXiv: 1612.05949 [astro-ph.HE].

[18] M. G. Aartsen et al. “Search for neutrinos from decaying dark matter with IceCube”. In: *Eur. Phys. J.* C78.10 (2018), p. 831. DOI: 10.1140/epjc/s10052-018-6273-3. arXiv: 1804.03848 [astro-ph.HE].

[19] A. Albert et al. “Search for Dark Matter Annihilation in the Earth using the ANTARES Neutrino Telescope”. In: *Phys. Dark Univ.* 16 (2017), pp. 41–48. DOI: 10.1016/j.dark.2017.04.005. arXiv: 1612.06792 [hep-ex].

[20] A. D. Avrorin et al. “Dark matter constraints from an observation of dSphs and the LMC with the Baikal NT200”. In: *J. Exp. Theor. Phys.* 125.1 (2017). [Zh. Eksp. Teor. Fiz.152,no.1,97(2017)], pp. 80–90. DOI: 10.1134/S1063776117070135. arXiv: 1612.03836 [astro-ph.HE].

[21] T Tanaka et al. “An indirect search for weakly interacting massive particles in the sun using 3109.6 days of upward-going muons in Super-Kamiokande”. In: *The Astrophysical Journal* 742.2 (2011), p. 78.

[22] K Choi et al. “Search for neutrinos from annihilation of captured low-mass dark matter particles in the Sun by Super-Kamiokande”. In: *Physical review letters* 114.14 (2015), p. 141301.

[23] Andrew Gould. “Resonant Enhancements in WIMP Capture by the Earth”. In: *Astrophys. J.* 321 (1987), p. 571. DOI: 10.1086/165653.

[24] Giacomo Beccari and Giovanni Carraro. “Introduction to the Theory of Stellar Evolution”. In: *Ecology of Blue Straggler Stars*. Springer, 2015, pp. 1–16.

[25] Katherine Freese et al. “Stellar structure of dark stars: A first phase of stellar evolution resulting from dark matter annihilation”. In: *The Astrophysical Journal Letters* 685.2 (2008), p. L101.

[26] Katherine Freese. “Review of Observational Evidence for Dark Matter in the Universe and in upcoming searches for Dark Stars”. In: *EAS Publ. Ser.* 36 (2009), pp. 113–126. DOI: 10.1051/eas/0936016. arXiv: 0812.4005 [astro-ph].

[27] Katherine Freese, Douglas Spolyar, and Anthony Aguirre. “Dark Matter Capture in the first star: a Power source and a limit on Stellar Mass”. In: *JCAP* 0811 (2008), p. 014. DOI: 10.1088/1475-7516/2008/11/014. arXiv: 0802.1724 [astro-ph].

[28] Katherine Freese et al. “Dark Stars: A Review”. In: *Rept. Prog. Phys.* 79.6 (2016), p. 066902. DOI: 10.1088/0034-4885/79/6/066902. arXiv: 1501.02394 [astro-ph.CO].

[29] Reinhard Genzel, Frank Eisenhauer, and Stefan Gillessen. “The Galactic Center massive black hole and nuclear star cluster”. In: *Reviews of Modern Physics* 82.4 (2010), p. 3121.

[30] AM Ghez et al. “Stellar orbits around the galactic center black hole”. In: *The Astrophysical Journal* 620.2 (2005), p. 744.

[31] A. M. Ghez et al. “The first measurement of spectral lines in a short - period star bound to the galaxy’s central black hole: A paradox of youth”. In: *Astrophys. J.* 586 (2003), pp. L127–L131. DOI: `10.1086/374804`. arXiv: `astro-ph/0302299 [astro-ph]`.

[32] J Zorec and F Royer. “Rotational velocities of A-type stars-IV. Evolution of rotational velocities”. In: *Astronomy & Astrophysics* 537 (2012), A120.

[33] Pierre Salati. “A stellar probe of dark matter annihilation in galactic nuclei”. In: *Dark Matter: Proceedings of the XXIIIrd Rencontre de Moriond, Les Arcs, Savoie, France, March 8-15, 1988, Series–Moriond Astrophysics Meetings*. Editions Frontières. 1988, p. 403.

[34] M. G. Aartsen et al. “Improved limits on dark matter annihilation in the Sun with the 79-string IceCube detector and implications for supersymmetry”. In: *JCAP* 1604.04 (2016), p. 022. DOI: `10.1088/1475-7516/2016/04/022`. arXiv: `1601.00653 [hep-ph]`.

[35] M. Ackermann et al. “Optical properties of deep glacial ice at the South Pole”. In: *J. Geophys. Res. Atmos.* 111.D13 (2006), p. D13203. DOI: `10.1029/2005JD006687`.

[36] Rasha Abbasi et al. “Calibration and characterization of the IceCube photomultiplier tube”. In: *Nuclear Instruments and Methods in Physics Research Section A: Accelerators, Spectrometers, Detectors and Associated Equipment* 618.1-3 (2010), pp. 139–152.

[37] R. Abbasi et al. “The IceCube Data Acquisition System: Signal Capture, Digitization, and Timestamping”. In: *Nucl. Instrum. Meth.* A601 (2009), pp. 294–316. DOI: `10.1016/j.nima.2009.01.001`. arXiv: `0810.4930 [physics.ins-det]`.

[38] Markus Ahlers and Francis Halzen. “Opening a new window onto the universe with IceCube”. In: *Progress in Particle and Nuclear Physics* (2018).

[39] M. G. Aartsen et al. “Energy Reconstruction Methods in the IceCube Neutrino Telescope”. In: *JINST* 9 (2014), P03009. DOI: `10.1088/1748-0221/9/03/P03009`. arXiv: `1311.4767 [physics.ins-det]`.

[40] C Amole et al. “Dark matter search results from the PICO-60 CF 3 I bubble chamber”. In: *Physical Review D* 93.5 (2016), p. 052014.

[41] C Amole et al. “Improved dark matter search results from PICO-2L Run 2”. In: *Physical Review D* 93.6 (2016), p. 061101.

[42] E Behnke et al. “Final results of the PICASSO dark matter search experiment”. In: *Astroparticle Physics* 90 (2017), pp. 85–92.

[43] M Felizardo et al. “The SIMPLE phase II dark matter search”. In: *Physical Review D* 89.7 (2014), p. 072013.

[44] Changbo Fu et al. “Spin-dependent weakly-interacting-massive-particle–Nucleon cross section limits from first data of PandaX-II experiment”. In: *Physical review letters* 118.7 (2017), p. 071301.

[45] Mark Gerald Aartsen et al. “Search for dark matter annihilations in the Sun with the 79-string IceCube detector”. In: *Physical review letters* 110.13 (2013), p. 131302.

[46] S. Adrian-Martinez et al. “Limits on Dark Matter Annihilation in the Sun using the ANTARES Neutrino Telescope”. In: *Phys. Lett.* B759 (2016), pp. 69–74. DOI: 10.1016/j.physletb.2016.05.019. arXiv: 1603.02228 [astro-ph.HE].

[47] K Choi et al. “Search for neutrinos from annihilation of captured low-mass dark matter particles in the Sun by Super-Kamiokande”. In: *Physical review letters* 114.14 (2015), p. 141301.

[48] DS Akerib et al. “Results from a search for dark matter in the complete LUX exposure”. In: *Physical review letters* 118.2 (2017), p. 021303.

[49] Andi Tan et al. “Dark matter results from first 98.7 days of data from the PandaX-II experiment”. In: *Physical review letters* 117.12 (2016), p. 121303.

[50] E Aprile et al. “XENON100 dark matter results from a combination of 477 live days”. In: *Physical Review D* 94.12 (2016), p. 122001.

[51] Marc Kamionkowski and Ali Kinkhabwala. “Galactic halo models and particle dark matter detection”. In: *Phys. Rev.* D57 (1998), pp. 3256–3263. DOI: 10.1103/PhysRevD.57.3256. arXiv: hep-ph/9710337 [hep-ph].

[52] E. E. Mamajek et al. “IAU 2015 Resolution B3 on Recommended Nominal Conversion Constants for Selected Solar and Planetary Properties”. In: (2015). arXiv: 1510.07674 [astro-ph.SR].

[53] Yoshiaki Sofue. “Rotation Curve and Mass Distribution in the Galactic CenterâFrom Black Hole to Entire Galaxyâ”. In: *Publications of the Astronomical Society of Japan* 65.6 (2013), p. 118.

[54] Aldo Serenelli et al. “New Solar Composition: The Problem With Solar Models Revisited”. In: *Astrophys. J.* 705 (2009), pp. L123–L127. DOI: 10.1088/0004-637X/705/2/L123. arXiv: 0909.2668 [astro-ph.SR].

[55] Francesc Ferrer and Daniel R Hunter. “The impact of the phase-space density on the indirect detection of dark matter”. In: *Journal of Cosmology and Astroparticle Physics* 2013.09 (2013), p. 005.

[56] Riccardo Catena and Bodo Schwabe. “Form factors for dark matter capture by the Sun in effective theories”. In: *JCAP* 1504.04 (2015), p. 042. DOI: 10.1088/1475-7516/2015/04/042. arXiv: 1501.03729 [hep-ph].

[57] Aaron C Vincent, Pat Scott, and Aldo Serenelli. “Updated constraints on velocity and momentum-dependent asymmetric dark matter”. In: *Journal of Cosmology and Astroparticle Physics* 2016.11 (2016), p. 007.

[58] Paweł Haensel, Aleksander Yu Potekhin, and Dmitry G Yakovlev. *Neutron stars 1: Equation of state and structure*. Vol. 326. Springer Science & Business Media, 2007.

[59] Chris Kouvaris. “WIMP Annihilation and Cooling of Neutron Stars”. In: *Phys. Rev.* D77 (2008), p. 023006. DOI: 10.1103/PhysRevD.77.023006. arXiv: 0708.2362 [astro-ph].

[60] Joseph Bramante, Keita Fukushima, and Jason Kumar. “Constraints on bosonic dark matter from observation of old neutron stars”. In: *Phys. Rev.* D87.5 (2013), p. 055012. DOI: 10.1103/PhysRevD.87.055012. arXiv: 1301.0036 [hep-ph].

[61] Joseph Bramante and Tim Linden. “Detecting Dark Matter with Imploding Pulsars in the Galactic Center”. In: *Phys. Rev. Lett.* 113.19 (2014), p. 191301. DOI: 10.1103/PhysRevLett.113.191301. arXiv: 1405.1031 [astro-ph.HE].

[62] NASA. "Solar System Exploration". In: ().

[63] G. G. Pavlov et al. "Detection of X-ray Emission from the Very Old Pulsar J0108-1431". In: *Astrophys. J.* 691 (2009), pp. 458–464. DOI: `10.1088/0004-637X/691/1/458`. arXiv: `0803.0761 [astro-ph]`.

[64] Jason WT Hessels et al. "A radio pulsar spinning at 716 Hz". In: *Science* 311.5769 (2006), pp. 1901–1904.

[65] William Wilson Morgan and Philip Childs Keenan. "Spectral classification". In: *Annual Review of Astronomy and Astrophysics* 11.1 (1973), pp. 29–50.

[66] Georges Meynet and A. Maeder. "Stellar evolution with rotation X: Wolf-Rayet star populations at solar metallicity". In: *Astron. Astrophys.* 404 (2003), pp. 975–990. DOI: `10.1051/0004-6361:20030512`. arXiv: `astro-ph/0304069 [astro-ph]`.

[67] J Silaj et al. "The Hα profiles of Be shell stars". In: *The Astrophysical Journal* 795.1 (2014), p. 82.

[68] Gerard T Van Belle and Kaspar Von Braun. "Directly determined linear radii and effective temperatures of exoplanet host stars". In: *The Astrophysical Journal* 694.2 (2009), p. 1085.

[69] AA Tokovinin. "MSC-a catalogue of physical multiple stars". In: *Astronomy and Astrophysics Supplement Series* 124.1 (1997), pp. 75–84.

[70] ML Malagnini and C Morossi. "Accurate absolute luminosities, effective temperatures, radii, masses and surface gravities for a selected sample of field stars". In: *Astronomy and Astrophysics Supplement Series* 85 (1990), pp. 1015–1019.

[71] Harold A. McAlister et al. "First results from the CHARA Array. 1. An Interferometric and spectroscopic study of the fast rotator Alpha Leonis (Regulus)". In: *Astrophys. J.* 628 (2005), pp. 439–452. DOI: `10.1086/430730`. arXiv: `astro-ph/0501261 [astro-ph]`.

[72] K. Griest and D. Seckel. "Cosmic Asymmetry, Neutrinos and the Sun". In: *Nucl. Phys.* B283 (1987). [Erratum: Nucl. Phys.B296,1034(1988)], pp. 681–705. DOI: `10.1016/0550-3213(87)90293-8,10.1016/0550-3213(88)90409-9`.

[73] Andrew Gould. "{WIMP} Distribution in and Evaporation From the Sun". In: *Astrophys. J.* 321.SLAC-PUB-4162 (1987), p. 560.

[74] Andrew Gould. "Evaporation of WIMPs with arbitrary cross sections". In: *The Astrophysical Journal* 356 (1990), pp. 302–309.

[75] Giorgio Busoni et al. "Evaporation and scattering of momentum- and velocity-dependent dark matter in the Sun". In: *JCAP* 1710.10 (2017), p. 037. DOI: `10.1088/1475-7516/2017/10/037`. arXiv: `1703.07784 [hep-ph]`.

[76] Andrzej K Drukier, Katherine Freese, and David N Spergel. "Detecting cold dark-matter candidates". In: *Physical Review D* 33.12 (1986), p. 3495.

[77] Jürg Diemand and Ben Moore. "The structure and evolution of cold dark matter halos". In: *Advanced Science Letters* 4.2 (2011), pp. 297–310.

[78] Carlos S Frenk and Simon DM White. "Dark matter and cosmic structure". In: *Annalen der Physik* 524.9-10 (2012), pp. 507–534.

[79] Julio F. Navarro, Carlos S. Frenk, and Simon D. M. White. "The Structure of cold dark matter halos". In: *Astrophys. J.* 462 (1996), pp. 563–575. DOI: `10.1086/177173`. arXiv: `astro-ph/9508025 [astro-ph]`.

[80] Jaan Einasto. “On the Construction of a Composite Model for the Galaxy and on the Determination of the System of Galactic Parameters”. In: *Trudy Astrofizicheskogo Instituta Alma-Ata* 5 (1965), pp. 87–100.

[81] Julio F. Navarro et al. “The Inner structure of Lambda-CDM halos 3: Universality and asymptotic slopes”. In: *Mon. Not. Roy. Astron. Soc.* 349 (2004), p. 1039. DOI: 10.1111/j.1365-2966.2004.07586.x. arXiv: astro-ph/0311231 [astro-ph].

[82] Alister W. Graham et al. “Empirical models for Dark Matter Halos. I. Nonparametric Construction of Density Profiles and Comparison with Parametric Models”. In: *Astron. J.* 132 (2006), pp. 2685–2700. DOI: 10.1086/508988. arXiv: astro-ph/0509417 [astro-ph].

[83] Andreas Burkert. “The structure of dark matter halos in dwarf galaxies”. In: *The Astrophysical Journal Letters* 447.1 (1995), p. L25.

[84] Paolo Salucci et al. “Dwarf spheroidal galaxy kinematics and spiral galaxy scaling laws”. In: *Monthly Notices of the Royal Astronomical Society* 420.3 (2012), pp. 2034–2041.

[85] F Royer et al. “Rotational velocities of A-type stars in the northern hemisphere. II. Measurement of v sin i”. In: *Astronomy and Astrophysics* 393 (2002), pp. 897–911.